AD_____

GRANT NUMBER DAMD17-94-J-4511

TITLE: Real-Time 3-D Ultrasonic Diagnostic Imager for Battlefield Application

PRINCIPAL INVESTIGATOR: Timothy White, Anthony M. Nicoli, Kenneth Erikson

CONTRACTING ORGANIZATION: LORAL Infrared and Imaging Systems
Lexington, Massachusetts 02173

REPORT DATE: October 1996

TYPE OF REPORT: Annual

PREPARED FOR: Commander
U.S. Army Medical Research and Materiel Command
Fort Detrick, Frederick, Maryland 21702-5012

DISTRIBUTION STATEMENT: Approved for public release;
distribution unlimited

DISCLAIMER NOTICE

THIS DOCUMENT IS BEST QUALITY AVAILABLE. THE COPY FURNISHED TO DTIC CONTAINED A SIGNIFICANT NUMBER OF PAGES WHICH DO NOT REPRODUCE LEGIBLY.

REPORT DOCUMENTATION PAGE

Form Approved
OMB No. 0704-0188

1. AGENCY USE ONLY (*Leave blank*)	2. REPORT DATE	3. REPORT TYPE AND DATES COVERED
	October 1996	Annual (1 Oct 95 - 30 Sep 96)

4. TITLE AND SUBTITLE
Real-Time 3-D Ultrasonic Diagnostic Imager for Battlefield Applications

5. FUNDING NUMBERS
DAMD17-94-J-4511

6. AUTHOR(S)
Mr. Timothy White, Mr. Anthony M. Nicoli, Mr. Kenneth Erikson

7. PERFORMING ORGANIZATION NAME(S) AND ADDRESS(ES)
LORAL Infrared and Imaging Systems
Lexington, Massachusetts 02173

8. PERFORMING ORGANIZATION REPORT NUMBER
9611-12

9. SPONSORING/MONITORING AGENCY NAMES(S) AND ADDRESS(ES)
U.S. Army Medical Research and Materiel Command
Fort Detrick, Maryland 21702-5012

10. SPONSORING/MONITORING AGENCY REPORT NUMBER

11. SUPPLEMENTARY NOTES
The views, opinions, and/or findings contained in this report are those of the authors and should not be construed as an official Department of the Army position, policy, or decision unless so designated by other documentation.

12a. DISTRIBUTION/AVAILABILITY STATEMENT
Approval for public release; distribution unlimited

12a. DISTRIBUTION CODE

13. ABSTRACT *(Maximum 200 words)*

This report presents progress achieved through the first 12 months of Phase II of a two-phase, 36 month technology development program.
During Phase I, Lockheed Martin demonstrated ultrasound imaging at 5 MHz using an electronically scanned, two-dimensional hybrid transducer array and an acoustic lens. The hybrid array was constructed by mating a readout integrated circuit (ROIC) originally designed for infrared imaging to a 44 x 64 element piezoelectric array.
Thus far in Phase II, Lockheed Martin has carried the design of a laboratory demonstration model of a battlefield ultrasonic imager completely through the preliminary design phase. The bistatic imager has two major subassemblies: the probe and the console. The probe acts as the ultrasonic transceiver, comprising the ultrasonic transmitters, a two element acoustic lens, a 128x 128 two-dimensional, transducer hybrid receive array, associated support electronics and mechanical assemblies. The console acts as the support and processing unit comprising a custom signal processor, an image processor, a high resolution analog video display, and other support equipment.
The laboratory demonstration model is planned to produce real-time (30 Hz), two-dimensional images with 1 mm resolution in three dimensions, and will be capable of real-time collection of three-dimensional data for volume rendering.

14. SUBJECT TERMS	15. NUMBER OF PAGES
Ultrasound, 3D Imaging, 2D Array, Medical Imaging, Portable	101
	16. PRICE CODE

17. SECURITY CLASSIFICATION OF REPORT	18. SECURITY CLASSIFICATION OF THIS PAGE	19. SECURITY CLASSIFICATION OF ABSTRACT	20. LIMITATION OF ABSTRACT
Unclassified	Unclassified	Unclassified	Unlimited

FOREWORD

Opinions, interpretations, conclusions and recommendations are those of the author and are not necessarily endorsed by the US Army.

✓ Where copyrighted material is quoted, permission has been obtained to use such material.

✓ Where material from documents designated for limited distribution is quoted, permission has been obtained to use the material.

✓ Citations of commercial organizations and trade names in this report do not constitute an official Department of Army endorsement or approval of the products or services of these organizations.

NA In conducting research using animals, the investigator(s) adhered to the "Guide for the Care and Use of Laboratory Animals," prepared by the Committee on Care and Use of Laboratory Animals of the Institute of Laboratory Resources, National Research Council (NIH Publication No. 86-23, Revised 1985).

NA For the protection of human subjects, the investigator(s) adhered to policies of applicable Federal Law 45 CFR 46.

NA In conducting research utilizing recombinant DNA technology, the investigator(s) adhered to current guidelines promulgated by the National Institutes of Health.

NA In the conduct of research utilizing recombinant DNA, the investigator(s) adhered to the NIH Guidelines for Research Involving Recombinant DNA Molecules.

NA In the conduct of research involving hazardous organisms, the investigator(s) adhered to the CDC-NIH Guide for Biosafety in Microbiological and Biomedical Laboratories.

Timothy E White

PI - Signature Date

TABLE OF CONTENTS

INTRODUCTION

This program seeks to apply a solid state, staring, ultrasonic hybrid array to demonstrate the first real-time, portable, C-scan diagnostic ultrasound medical imaging system with three-dimensional (3-D) capability for battlefield and trauma care.

Current B-scan ultrasound imaging limits the visualization of 3-D structures because only 2-D slices are imaged. These slices must then be reconstructed in the operator's mind to obtain a mental 3-D "picture" of the target anatomy. Automatic movement of the transducer with computer reconstruction (off line) has recently been introduced by some manufacturers, but the systems are slower, more costly, and harder to use than conventional B-scan imaging instruments. They are not well suited to battlefield use.

Recognizing the importance of 3-D imaging, the ultrasound industry is in search of a technical solution to building high resolution, 2-D ultrasound arrays. The Lockheed Martin IR Imaging Systems solution is unique. It consists of constructing large imaging ultrasound arrays using processes derived from DARPA supported technology for infrared focal plane arrays (IRFPAs). We have directly applied existing designs and processes from thermal imaging systems to prove our ultrasound imaging capability.

This technology bridges the large gap between taking vital signs and making basic observations in the field and taking CT scans back in a hospital. With C-scan technology brought to the field, deep tissue damage assessment is done quickly, enabling earlier intervention. This is true for either battlefield environments or EMT/ambulance applications. Real-time imagery also affords the opportunity for transmission, remote diagnosis, and archiving of information. This can also benefit health care in remote locations where specialists and expensive imaging diagnostic equipment are not available.

Earlier efforts had already proven the feasibility of the 2-D transducer hybrid array. We successfully imaged the direct illumination of a focused source with our 44x64 element transducer array technology. We believe this 44 x 64 element ultrasound array to be the largest operating two dimensional (2-D) ultrasound array in existence.

During Phase I of this project, our goal was to demonstrate real-time C-scan imagery from reflecting targets. Our approach was to build 2-D ultrasonic hybrid transducers using a diced array of piezoelectric elements mated to an existing readout integrated circuit (ROIC). We also modified existing hardware to enable the capture and analysis of real time C-scan imagery. To accomplish this, we modified an existing IR camera to provide range gate and timing controls necessary for ultrasonography. In parallel with this effort, and in support of the real-time imagery Phase I goal, the IRFPA-FM program established a transducer fabrication capability based on our IR read out integrated circuit and infrared focal plane fabrication technology.

As described in the October 1995 report, the Phase I effort demonstrated the feasibility of an ultrasonic battlefield imager using 2-D hybrids as the ultrasonic transducer by imaging reflected energy from both specular and diffuse scattering targets. An image of line targets, taken by the Phase I transducer hybrid is shown in Figure 1. This image presents a series of line targets buried within a medical ultrasound test object.

This report describes the work performed in the first half of Phase II with emphasis on the key design accomplishments, together with the challenges overcome. Our Phase II program builds on the success of the initial feasibility components developed in Phase I. We believe our approach will aid in

the location of foreign object fragments, the location and quantification of the extent of hemorrhage, and will improve techniques for guided surgery and biopsy.

The objective of Phase II of the BUDI program is to demonstrate a prototype ultrasonic imager capable of high quality ultrasound imagery suitable for 3D reconstruction. Phase II is a two year effort. This report covers the first year of that two year period. The plan for this year was to design and begin fabrication of a bi-static ultrasound imager employing a 128x128 receive array and multiple broad area transmitters to insonify the area of interest. The system incorporates a physical beam former (ultrasonic lens), receive array, custom electronics to operate the array and control system timing, a signal processor for image construction and a commercially available PC (personal computer) as the user interface. A separate high resolution video monitor, transmit transducers, and power amplifier complete the system. All portions of this system were analyzed to assure that the prototype could meet the performance requirements listed in Table 1.

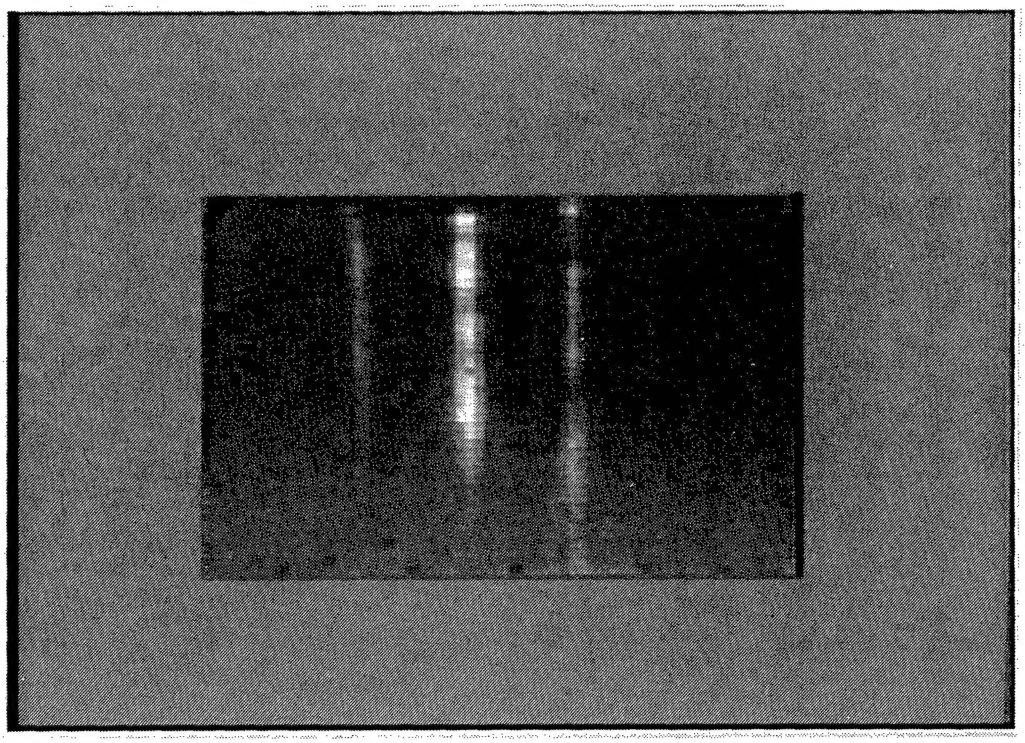

Figure 1. Image of 1 mm Monofilament Nylon in Tissue Equivalent Test Object at a Depth of 1 cm.

Table 1. System Target Requirements

Target Anatomy:		Abdominal Organs and Foreign Objects	
Frame Rate:		10 Hz - 30 Hz	
		BUDI	Present Systems
Resolution:	Azimuth:	1 mm	<2 mm
	Elevation:	1 mm	<6 mm
	Range:	1 mm	<0.5 mm
Operating Frequency:		5 MHz	
Penetration Depth:		15 cm	
Sensitivity:		9.7 μV/Pa; -220 dB re 1 V/μPa	
Noise Equivalent Pressure:		1.03 Pa	
Dynamic Range:		90 dB Total, >30 dB Instantaneous	
Fixed Pattern Noise:		1 LSB @ 8 bits or -48 dB re Max Level	

The schedule for Phase II is shown in Figure 2. The first three months of Phase II were dedicated to system trade-offs and system performance analysis. The second quarter was directed at establishing the system preliminary design with the primary focus being the establishment of the readout integrated circuit (ROIC) preliminary design. This long lead item is the electronic heart of the system. Its operating characteristics determined the characteristics of the remainder of the electronics and therefore warranted acceleration with respect to other system components. In July, the completed design was released to the foundry for fabrication. The anticipated completion date is December 3.

Upon solidification of the ROIC design, the detailed design of the remainder of the electronics was released. System electronics will begin delivery in December to facilitate ROIC testing and to expedite the integration process. Transducer arrays will be hybridized to the ROICs to make transducer hybrid assemblies (THAs) in the period January through May, with minor process and material variations to determine the optimum configuration. Finally, the period June through September will be allocated to operation and evaluation of the system at the University of Rochester with clinical evaluations at the University's Medical Center.

The following sections describe in detail the accomplishments to date in this phase of the contract.

SCIENTIFIC & TECHNICAL MERIT

The goals of our medical ultrasound imaging system development are visualization of the interior of a human subject with:

- Excellent image quality
- Real-time frame rates
- Image manipulation to obtain any derived view or cross-section
- Portability
- Low cost

Demonstration of imaging with a 16,384 element ultrasonic hybrid array will enable true real-time volumetric imaging with ultrasound.

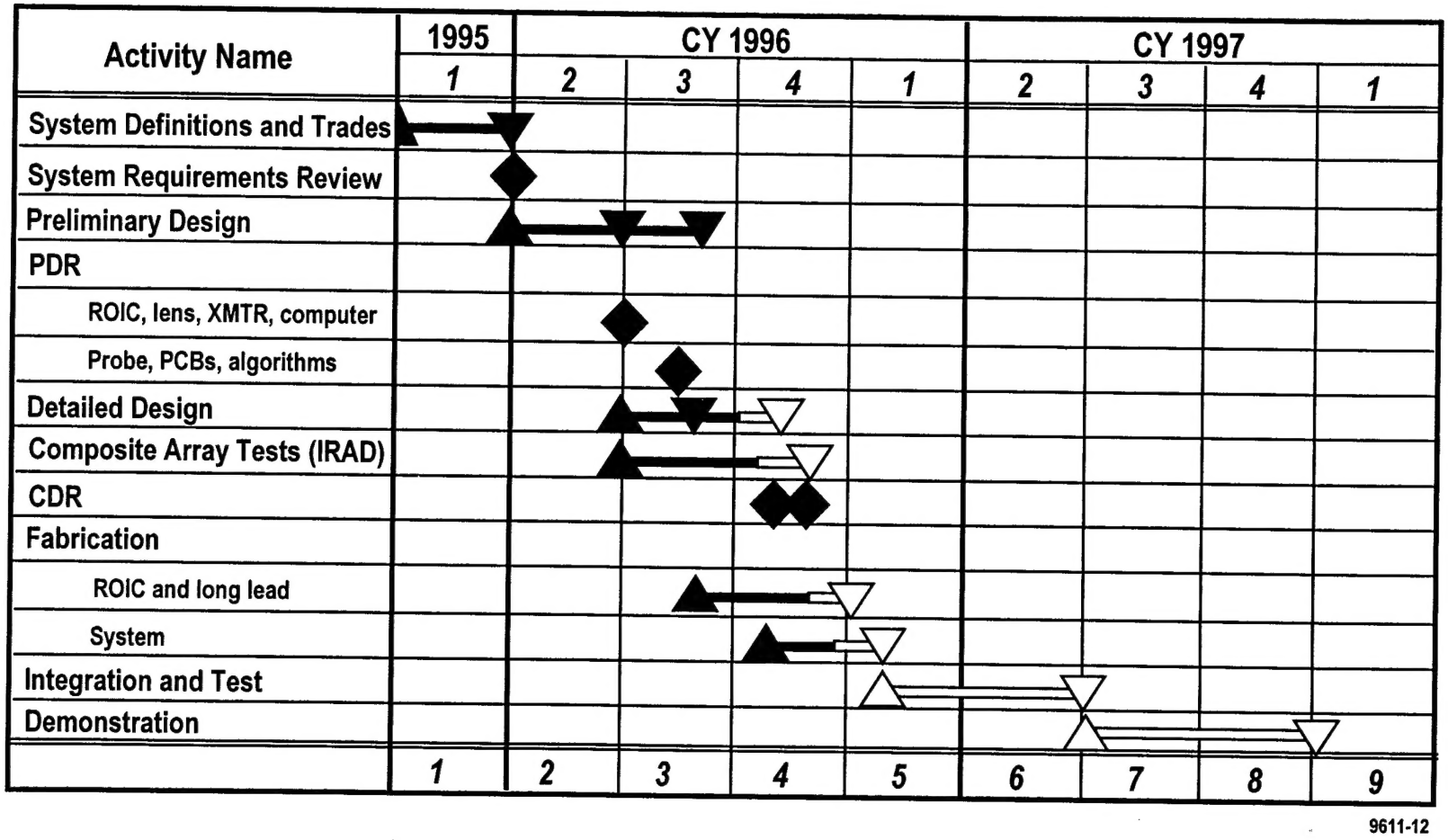

Figure 2. Phase II Schedule

RELEVANCE TO DARPA

Our imaging ultrasound array is the application of dual use technology derived from DARPA sponsored developments. Arrays are derived from IRFPA technology, using acoustically sensitive materials in place of the IR detectors. Under the flexible manufacturing program with DARPA/MTO, Lockheed Martin has also demonstrated fabrication of ultrasound hybrid arrays. By using the same IR hybrid fabrication line that supplies DoD and commercial IR imaging products, ultrasound arrays have been made available to this program without significant additional startup expenses, providing maximum synergy of DARPA activities.

CAPABILITIES AND COMMERCIALIZATION

We have assembled a team that includes key leaders in diagnostic ultrasound medicine, equipment development, and imaging systems:

- *University of Rochester, Center for Biomedical Ultrasound:* Dr. Kevin Parker, Director. The center is the oldest and largest interdisciplinary research organization in the world devoted to all aspects of medical imaging.
- *Lockheed Martin IR Imaging Systems:* A leader in military and commercial application of electro-optic imaging technologies, LIRIS will design and fabricate the ultrasonic imaging arrays and associated electronics.

We have had discussions with representatives of ATL, Siemans, Acuson, and GE. It is Lockheed Martin's intention to enter into an OEM agreement with a major system manufacturer to bring the product to market most effectively.

BUDI PHASE II IMAGER DESIGN AND OPERATION

The Real Time 3-D Battlefield Ultrasonic Diagnostic Imager (BUDI) is intended for imaging radiolucent shrapnel, fluid collections and abdominal organs under battlefield conditions. It will allow forward echelon personnel to perform more accurate and effective triage in order to evacuate the wounded who would most benefit. The Phase II Laboratory Demonstration System discussed in this Annual Report is under development at Lockheed Martin IR Imaging Systems and is intended only for use in a hospital IRB-controlled environment.

SYSTEM REQUIREMENTS

The Battlefield Ultrasonic Diagnostic Imager Laboratory Demonstration System (BUDI-LDS) seeks to image abdominal organs and pooled fluids in the abdominal cavity with dimensions greater than 1 cm, and hard objects within the abdomen, e.g. plastic or metal fragments, larger than 1 mm^3.

The system performance objectives are spatial resolution of 1 mm in all three spatial dimensions, an image dynamic range of greater than 30 dB at any single depth, a minimum resolvable contrast difference of 3 dB relative to the background level for small targets, and the ability to image from the skin's surface to a depth of 10 cm with full dynamic range, and to a depth of 15 cm for hard objects. The BUDI-LDS will provide a real-time, two-dimensional image, where real-time is defined as 30 frames per second.

The BUDI-LDS will also acquire data for subsequent three-dimensional image reconstruction and rendering. This data can take the form of either a sequence of frames focused at succeeding depths for direct volume rendering, or an amplitude and phase image from which three-dimensional data can be holographically reconstructed and subsequently rendered.

BUDI-LDS Top-Level Description

The Battlefield Ultrasonic Diagnostic Imager Laboratory Demonstration System (BUDI-LDS) consists of two major subsystems: the probe and the console, as shown in Figure 3.

The probe acts as the imaging transceiver. It generates the acoustic energy pulse required to interrogate the body using stand-alone transmit transducers. The probe is equipped with four, 5 MHz transmit transducers to allow the system to compose varying speckle patterns by changing the source of the ultrasonic pulse. The probe also collects and images the reflected ultrasonic return using an acoustic lens. The probe converts the ultrasonic image to electronic form using the acoustic imaging module (AIM).

The AIM consists of two subassemblies: the transducer hybrid assembly (THA) and the interface electronics (IE). The THA performs the acoustic to electronic image conversion. It resides in the focal plane of the acoustic lens, and consists of a 128x128 element, two-dimensional, piezoelectric array, electrically interconnected to a custom, silicon readout-integrated-circuit (ROIC). The interface electronics operates the THA, providing power and logic control signals. It also preprocesses the electronic image, and transfers this image to the console for further processing. The IE also controls the transmission of the acoustic energy pulse.

The console provides all functions associated with overall system control, image processing, image display, user interface and system support. Its primary elements are an IBM PC compatible microcomputer, a high resolution monochrome monitor, an RF power amplifier, and power conditioning electronics.

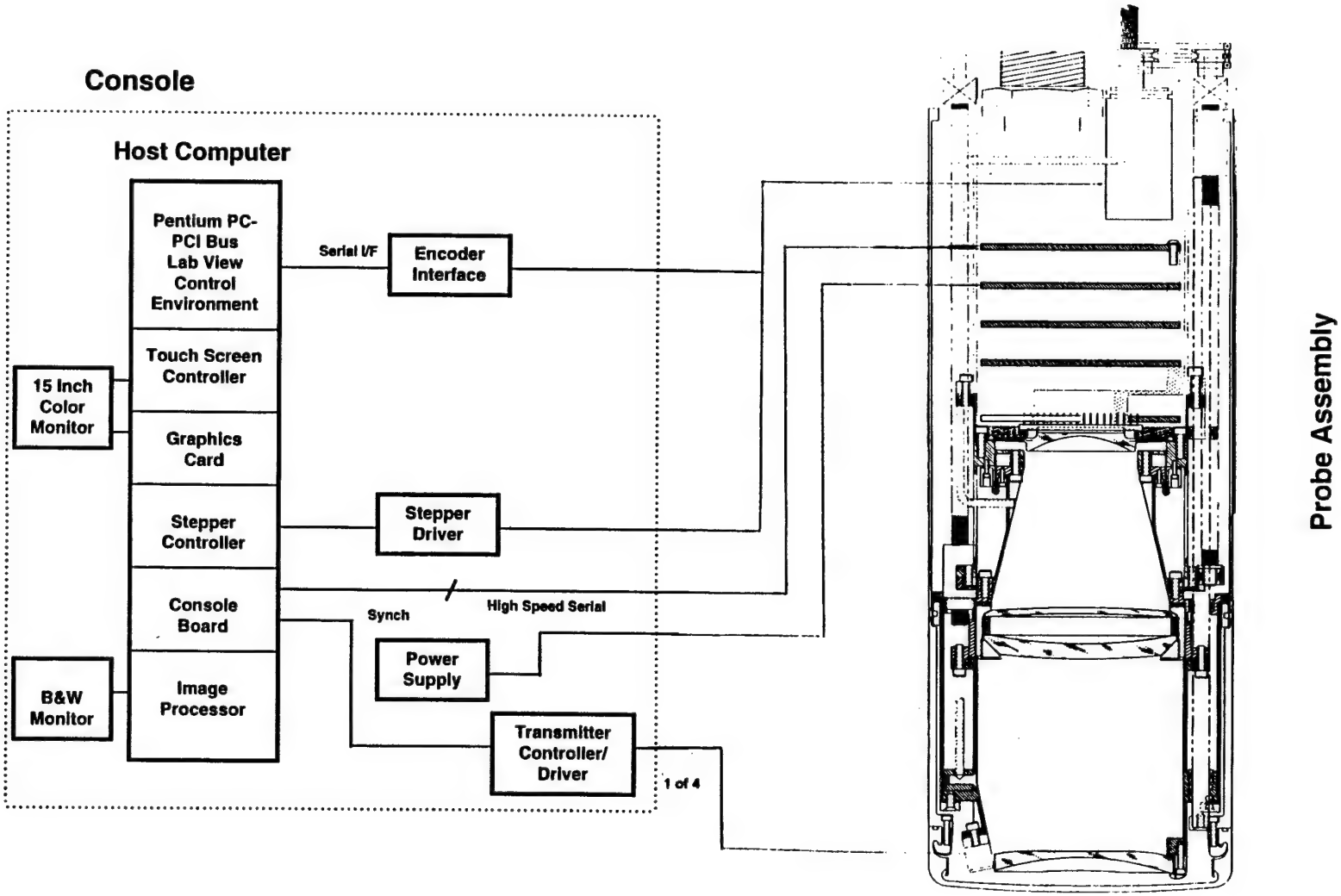

Figure 3. Battlefield Ultrasonic Diagnostic Imager (BUDI) Laboratory Demonstration System

The IBM PC compatible computer acts as the host CPU. It houses a custom digital signal processing board, the console board, a custom image memory board, the memory board, and a commercial-off-the shelf image processor. It provides a graphical user interface that allows the user to control image acquisition and display.

The console board runs embedded firmware to process AIM data into a two-dimensional image. It also acquires and stores AIM data using the memory board. The image processor applies image enhancement algorithms to improve displayed image quality and converts the digital image stream to analog video (RS-170) for presentation on a standard monitor.

The high resolution, monochrome monitor provides a high quality display of the final image. This monitor exceeds the performance of the standard broadcast receiver in that it supports contrast resolution of 32 gray levels.

The RF power amplifier supplies the required high power (up to 2500 W peak, into 50 ohms), high frequency pulses required for acoustic interrogation. It is controlled by the probe interface electronics and drives the transmit transducers.

Finally, the power conditioning electronics provides the primary low voltage power for the probe. It also contains an isolation transformer to eliminate shock hazards to operators and patients, as required by safety regulations.

BUDI-LDS FUNCTIONAL DESCRIPTION

The following functional description follows the "information" flow from the user through the host CPU to the transmitter/receiver and signal processing, through to visual display. It is intended to complement the physical description which follows this narrative.

System master control originates at the host CPU, which has display screens running under Windows 3.11 and LabView 4.0 on a conventional color monitor. The user selects a command such as START imaging from the User Interface screen using a trackball. This initiates setup information which is downloaded across an RS-485 serial port into the Interface Electronics (I/E) which is contained in the Acoustic Imaging Module (AIM).

The Interface Electronics interpret this command and begin image generation and acquisition. A 5 MHz gated sinewave signal and a synch signal are sent out to drive an external RF power amplifier. The high power RF pulse returns to the AIM and I/E, where it is distributed to one of four transmitter transducers.

A transmitter transducer converts the electrical pulse into an acoustic pulse, typically 100 to 200 μs in duration. This acoustic pulse propagates through an internal fluid path in the probe, and exits the probe through a low loss, low reflection acoustic window into the patient.

Without going into a detailed discussion of acoustic propagation in the human body, the following is a greatly simplified conceptual model of the body useful for ultrasonic imaging of radiolucent shrapnel embedded in the liver. The key components are:

1. The body wall consisting of layers of skin, muscle, and fat.

2. The liver consisting of a thin, fibrous capsule surrounding essentially homogeneous parenchymal tissue, interpenetrated by vessels of various sizes and directions.

3. The embedded material, assumed to have rough surfaces, sharp edges and to be approximately 1 cm in diameter.

Acoustically the body wall is a source of multiple reflections (reverberation) as well as scattering and refraction from the fat and muscle layers. The net result of passing a sound pulse through such a layer is a severely scrambled wavefront, which is often referred to as aberration. It is akin to the atmospheric distortion seen by a telescope when viewing a star.

Passing into the liver itself, the sound pulse experiences significant attenuation through absorption and scattering, typically -5 dB per cm path length. Larger vessels can produce large amplitude specular reflections, whereas small structures (small compared to a wavelength of the sound, $\lambda = 0.3$ mm) are generally unresolved and contribute to speckle noise in the final image.

The embedded shrapnel presents a randomly varying target to the ultrasound beam, depending on its orientation and surface characteristics. Typical target strengths are -30 to -50 dB re a perfect reflector.

Leaving the body, the sound reenters the acoustic window into the waterpath environment of the probe. A multi-element acoustical lens images one plane in the body onto an ultrasonic detector array. This lens is diffraction limited and is optimized for the acoustic frequency and focal plane array dimensions.

A Transducer Hybrid Array (THA) consisting of a 128x128 (16,384 total elements) composite piezoelectric array, flip chip bonded directly to four very large custom silicon read-out integrated circuits (ROIC) is used to detect and readout the focused image. Up to 5 range gates are used to activate the THA for the few microseconds when the acoustic pulse from the object plane is present.

The I/E electronics provide the control signals, clocks and power for the ROICs. Each acoustic element of the array is $2/3\lambda$ square and is bonded directly to a similarly sized region on the integrated circuit containing a preamplifier, analog sampling, signal processing and storage. The in-phase (I) and quadrature (Q) components of the ultrasonic image signals incident on the array from the single transmitted pulse are simultaneously sampled and stored on all 16,384 ROIC cells.

The sampled data stored in the four ROICs are then rastered out through 16 parallel, high-speed data channels into the I/E electronics, where they are digitized to 12 bits, ordered and multiplexed through four parallel high speed serial ports leading to the console board in the host CPU.

In the console board, data from the serial ports are converted back to 12 bit words and magnitude and phase are computed from the sampled I and Q components of the image.

These data are then sent over hardwired ports to an image processor (IP) board in the PC, where gain correction, median filtering, bilinear interpolation to 256x256, gray scale manipulation, and finally RS-170 formatting occurs. At this point, the video image is sent to a diagnostic quality 8 inch black and white monitor for operator viewing.

This completes the process for a single pulse of sound. Depending on the imaging configuration selected by the operator several additional operations may be performed. Two key operations will be described further.

First, the maximum transmitted pulse rate is determined by the time it takes the pulse to travel from the transmitter, pass through the acoustic window, enter and leave the body and propagate back through the acoustic lens to the THA. This time is determined by the velocity of sound in the various media and the path lengths traveled. For a 15 cm depth in the body, a 500 Hz rate is readily achieved. Since a video monitor updates its information at 30 Hz, this means that up to 16 acoustic frames can be averaged to improve image quality. For this averaging to be effective, any noise in the images must be statistically independent. One of the major image noise sources expected is ultrasonic speckle arising from the coherent nature of the ultrasound and the properties of the human body. To create images with statistically independent speckle noise, four spatially separated transmitting transducers, driven at multiple frequencies, are employed. These acoustic frames are then averaged in the console board.

The other key operation is to compensate for pixel to pixel variations in the system due to non-uniform insonification and spatial variations in lens transmission, array element sensitivity and ROIC amplifier gain and offset. This is also done in the console board through a real-time lookup table that is loaded off-line during system calibration.

Other available system features include storage of raw data on a hard disk or erasable optical disk, videotaping of the displayed images, as well as access to system parameters through an expert user/test interface.

BUDI-LDS Components

The following sections describe the components of the probe and console in greater detail. They discuss design considerations, requirements and implementation, and expected performance.

Probe Assembly — Appendix A describes the total probe assembly. The probe provides the mechanical configuration required to support the various subsystems of the imager, including the transmitter, the water-filled acoustic lens, the acoustic imaging module[1], and the lens focusing and object depth selection mechanism.

Figure A1 lists the key considerations included in the probe design process. Figure A2 represents the probe itself and indicates its major subassemblies. Figure A3 spells out designs trades conducted to achieve the present compact probe size, while controlling the fluid volume and keeping all electrical and most mechanical components outside the fluid volume.

Figure A4 depicts the probe at the extremes of the image depth range. Since the BUDI-LDS employs a fixed focused lens for simplicity, the probe shroud extends to image shallow depths. An external pump fills the additional fluid volume to provide a continuous image path.

Figure A5 describes the probe's depth and focus drives. The focus drive is used to allow optimal adjustment of the fixed-focus lens, while the depth drive allows the selection of the desired object plane.

[1] The AIM is composed of the Transducer Hybrid Assembly and circuit boards labeled in Figure A2.

Figure A6 details the interface between the acoustic lens and the THA. This interface is designed to provide both optimum acoustic matching and a robust water seal.

Transmitter Subsystem — Appendix B describes the transmitter subsystem. As depicted in Figure B1, it consists of the transmitter drive circuit board, an RF power amplifier, and four transmitter transducers. The probe houses the drive circuit and transducers, while the RF amplifier is contained within the console for this demonstration program. Figure B2 summarizes the key requirements of the transmitter.

The interface electronics controls transmitter operation during imaging, setting the transmitted frequency, synchronizing the output pulse with the operation of the THA, and selecting the transducer that will transmit during a given frame.

A pulse is initiated when the IE generates a gated, sinusoidal voltage pulse at the frequency of interest. The drive circuit receives this pulse, controls its amplitude, and passes it to the RF amplifier, where it receives a fixed gain. This increases the total power of the pulse to a maximum of 2500 W peak. The high power voltage pulse returns to the drive circuit, where a high power, high speed relay bank routes it to the selected transducer.

The transducer, shown in Figure B3, converts the pulse into ultrasonic energy, and emits it into the body. As shown in Figure B4, the transducer is designed to fill the entire 80 mm x 80 mm field of view of the acoustic lens.

Lens — Appendix C describes the acoustic lens. Figure C1 depicts the lens structure. It is a two element, fixed focus lens, employing a liquid filled second element. A zero-power acoustic window resides in front of the lens. The object plane is 150 mm ahead of this window.

The lens uses only two refractive materials, polystyrene and a Flourinert liquid. It incorporates four aspheric surfaces and two spherical surfaces to produce a 1.1 mm blur circle[2]. Figure C2 lists its physical and performance characteristics.

Figure C3 presents the lens point spread function (or circularly symmetric beam pattern) parametric with object field position. Figure C4 presents the extent of the point spread function measured at 10%, 1% and 0.1% relative to the central maximum. It is constant with field position and remains relatively narrow down to the 1% point.

Figure C5 presents two key trades that contributed to the design of the acoustic lens.

THA — The Transducer Hybrid Assembly forms the receive transducer for the BUDI-LDS. It consists of a 128 x 128 (16,384) element, two-dimensional array of piezoelectric transducers electrically integrated to a 128 x 128 element array of amplification and processing electronics. Figure D1 is a plan view of the THA, showing its final form. The piezoelectric array is attached to four 64 x 64 element readout integrated circuits, shown in Figure D2, using an indium bump bonding technique developed for infrared focal plane assembly. The resulting package is ~1.8" square and provides a 25.6 mm square active area. Figure D3 provides a cross sectional view of the THA. Note that the array active surface rises above the package top surface to mate with the membrane that forms the acoustic interface with the lens.

[2] The "blur circle" is defined here as the diameter of a circle in the image plane that encircles 85% of all rays emitted from an on-axis object point.

Array — Appendix E describes the piezoelectric array. This array forms the acoustic-to-electric transducer and is composed of a 1-3 composite piezoelectric material based on PZT-5H.

Figure E1 presents the physical and performance specifications for the array. It is composed of 128 x 128, 180 μm square piezoelectric elements, surrounded by a ground electrode, as shown in Figure E2. The array dimensions and matching layer are tuned to resonate at 5 MHz, and provide a minimum 2 MHz 6 dB-bandwidth. A sensitivity of greater than -212 dB re 1V/μPa is predicted, and nearest neighbor crosstalk rejection of greater than 30 dB is anticipated. Figure E3 is a detailed view of one composite structure. Here, each piezoelectric element contains four subelements.

Readout Integrated Circuit (ROIC) — Appendix F describes the readout integrated circuit. As described in Figure F1, the ROIC provides a 64 x 64 (4096) element (or unit cell) array of amplification and processing electronics. It also provides the required analog multiplexing and support electronics to readout this array at a rate of up to nearly 500 Hz using four outputs, each capable of providing up to 10 million analog samples per second.

Figure F2 presents the electrical signal chain within the ROIC, while Figure F3 presents the predicted electrical performance of the ROIC. Figure F4 is a rendering of the ROIC's unit cell. Each electrical subsystem is evident in this rendering.

The ROIC is capable of two data collection modes, as summarized in Figure F5. Mode 1 derives in-phase and quadrature (I/Q) data from the temporal voltage signal. This data is later converted to a magnitude and phase measurement of the voltage generated by each transducer element during the period of interest defined by the range gate width. The ROIC can store up to five separate I/Q data sets, using the five storage cell banks resident in each unit cell. This allows the BUDI-LDS to capture a three-dimensional data set, containing image data from up to five separate depths within the body, using a single acoustic pulse. Figure F6 graphically represents the five plane data format for this mode.

Mode 2 employs sample and hold circuits to digitally sample the voltage waveform. Up to 20 digital samples can be acquired per transmit pulse. These samples can be used derive a number of different values, e.g. peak value or rms average, appropriate for use in image display.

Figures F7 through F11 present the amplifier trade conducted during ROIC unit cell design, the electrical operating modes of the ROIC, and the predicted electrical performance for the ROIC, including total harmonic distortion, wideband noise, and electrical crosstalk.

System Electronics — The BUDI-LDS has three primary electronic subsystems that perform control and processing functions. They are the ROIC interface electronics, the console and memory boards, and the digital signal processing (DSP) image processing board. Figure G1 presents a block diagram of the functional relationships between these subsystems.

ROIC Interface Electronics (IE) — Figure G2 outlines the requirements for the interface electronics. The IE controls image acquisition and readout, from acoustic pulse transmission and data collection to analog multiplexing. It also preprocesses image data by combining quadrature data samples, and communicates image data to the console board over a high speed, 300 Mbytes/second, digital, fiber-channel interface.

Console & Memory Boards — Figure G3 lists the requirements for the console and memory boards. These boards compose image data into ordered 128 x 128 image frames, buffer image data for

digital recording and repetitive or "cine" playback, execute a variety of image processing algorithm functions and transmit processed high-speed image data to the DSP image processor.

Figure G4 presents a diagram of the processing algorithm applied to the image data by the console board when the ROIC is operated in quadrature sampling mode. Algorithmic functions include image composition, magnitude and phase calculation, plane display selection, frame averaging and data storage. Figure G6 also presents an estimate of processing throughput required to execute these functions.

Figure G5 presents a diagram of the processing algorithm applied to the image data by the console board when the ROIC is operated in digital sampling mode. Algorithmic functions include image composition, offset correction, displayed value calculation, frame averaging and data storage. Figure G5 also presents an estimate of processing throughput required to execute these functions. Figure G6 presents a hardware block diagram of the console board.

The frame averaging algorithm is applied to improve image signal-to-noise ratio by averaging uncorrelated image noise. One component of this noise is thermal noise originating at the transducer. However, a more significant component is speckle arising from the interference pattern generated by the coherent insonification of the object plane within the body. By varying the frequency of the emitted sonic pulse, and the point of origin of this pulse, from frame to frame, this speckle pattern becomes uncorrelated. Therefore, the frame averaging algorithm will reduce this uncorrelated noise source as well.

DSP Image Processor — The DSP image processing board is a commercially available DSP card built around the Analog Devices SHARC high-speed, floating point processing chip. This card will be programmed in C to execute the image enhancement algorithms presented in Figure G7. These algorithms include a gain correction algorithm to compensate for non-uniformities in transducer sensitivity and ROIC amplifier gain across the THA, image median filtering to remove single point image defects, two-dimensional bilinear interpolation to increase the displayed image to 256 x 256 from 128 x 128 to improve displayed image appearance, a gray scale manipulation lookup-table to provide end-users with a choice of image contrast settings, and RS-170 formatting to create an analog video signal suitable for display on a conventional monitor. These functions are applied in both ROIC operating modes.

Support Hardware — The remaining components of the BUDI-LDS are commercial off-the-shelf items. They include a IBM PC compatible microcomputer, a number of DC power supplies, an 8" high-resolution monitor, an equipment rack and a medical grade isolation transformer.

Software — The BUDI-LDS employs a variety of software to provide user interfaces, control functions, and processing functions. Figure H1 depicts the relationship among the various software objects and the hardware with which they interact.

Software objects resident on the IBM compatible host computer run under Windows 3.11, and are written either in C or in the National Instruments LabVIEW environment. LabVIEW was chosen to minimize the effort associated with creating a high quality graphical user interface for the BUDI-LDS.

Software objects resident on the DSP image processor are written in C, while the console board, memory board, and ROIC interface electronics are all run using on-board firmware.

CONCLUSIONS & STATUS

Phase II activities to date have resulted in a preliminary design for a complete ultrasonic imager based on a 2-D, receive only transducer hybrid assembly. At the close of the first year of Phase II, the BUDI-LDS stands ready for the completion of detailed design, the subsequent fabrication of components, and the integration of a working imager.

POINT SPREAD FUNCTION COMPARISON

The following section describes an experiment conducted to compare the point spread function (2D beam pattern) of the Lockheed Martin doublet acoustic lens with the point spread function (2D beam pattern) of a conventional B-scan ultrasound imager. This experiment revealed a dramatically smaller point spread function for the doublet lens when compared to the conventional B-scan linear phased array.*

* This work was funded by Lockheed Martin internal research and development funds. It appears here in support of the BUDI system concept.

Point Spread Function Comparison

Conventional High Performance Linear Phase Array Transducer compared to the BUDI Phase I Doublet Lens

Experiments performed at the University of Rochester

Dan Phillips, Xucai Chen, Kevin Parker, Ken Erikson

(Presented at 6/19/96 PDR)

Abstract

The point spread function is a measurement of an imaging system response to a point source or target. The PSF can be affected by the aperture through which the image is formed and the medium through which the waves forming the image propagate. Experiments were performed to assess the PSF of an acoustic doublet lens and a conventional linear phased array in response to a point target embedded in scattering and non-scattering material. It was found that the doublet lens had similar spatial resolution in the azimuthal direction and superior spatial resolution in the elevation direction. Due to the aperture geometry and one-way focusing, the doublet lens should exhibit a smaller angular extent of the sidelobes than the linear phased array. Noise floor limitations of the data acquisition system limited assessment of this.

Problem Statement

Conventional linear phased array transducers produce B-scan images comprised of signals reflected from structures that lie primarily in a plane described by the range and azimuthal axes. The acoustic doublet lens is being used to produce C-scan images comprised of signals reflected from structures that lie in a planes described by the elevational and azimuthal axes at specified ranges. The PSF of interest for these experiments is one measured in the C-scan imaging plane . In order to compare the PSF in the C-scan imaging plane for the doublet lens and the linear phased array transducer, a series of parallel linear phased array transducer (LPAT) B-scan images were acquired at evenly spaced elevational increments and then processed to produce equivalent C-scan images for comparison. The same targets were used to acquire image information for both the doublet lens and the LPAT.

Goal of Experiment

The goal of the experiment was to measure the point spread function of an acoustic doublet lens and a conventional linear phased array transducer in scattering and non-scattering media.

Targets

There were two targets that differed in the composition of the embedding material. In both targets, the point scatterer consisted of a 0.5mm diameter tungsten carbide sphere. One target consisted of a 0.5mm diameter tungsten carbide sphere embedded 40 mm from the circular surface of a 3% agar cylinder (AGAR). The cylinder had a 76.2 mm diameter and 90 mm height. The sphere was located along the central axis of the cylinder.

The other target consisted of a 0.5mm diameter tungsten carbide sphere embedded in a 100mm by 100mm by 88mm cube of tissue equivalent material (TEM) prepared by ATS Laboratories, Inc. of Bridgeport, CT. The material has a speed of sound equal to 1469 m/s, attenuation coefficient equal to 0.692 dB/cm/MHz and a backscatter coefficient equivalent to the AIUM standard for liver. The tungsten carbide sphere was positioned 21.9mm from the front of the cube, 30.7mm from the left side of the cube and 21.9mm from the bottom of the cube. The offset position of the sphere from the center of the cube enabled measurements involving differing depths of scattering material.

Experimental Equipment

Except as noted in the following, description of experimental equipment, procedures and data analysis can be found in the summary report entitled **Acoustic Lens Characterization in Scattering Medium** dated and presented toLockheed Martin (then LIRIS) on 18 March 1996.

Linear Phased Array

Description of Experiment

The images were acquired with an Acuson 128XP/10 imaging system using an L5 linear phased array transducer operating at 5MHz. The nominal dimensions of the transducer aperture were 43mm in the azimuthal direction and 6.5 mm in the elevation direction. The transducer was held in mechanical positioning system that allowed it to be scanned across the surface of the target material in precise 1mm increments in the elevation direction. (Figure 1)

For the non-scattering medium, the transducer was scanned in the elevational direction along the circular surface of the AGAR target. The 0.5mm tungsten carbide sphere was located 40mm from the scanning surface along the cylindrical axis. For the scattering medium, the transducer was scanned in the elevational direction along the left side of the TEM cube where the 0.5mm tungsten carbide sphere was located 31mm below the surface. In both cases, a thin coat of coupling gel was placed on the target and the transducer face. The transducer face was then placed in contact with the surface of the target material.

From a theoretical point of view, the beam pattern of the LPAT was modeled as a rectangular aperture, to a first approximation. The x-axis corresponds to the azimuthal direction and the y-axis to the elevational direction. The intensity in both directions was therefore modeled by a (sin(l)/l)^2 ("Sinc" squared) function where l = (width of aperture along axis of interest • distance along axis of interest from center) / (wavelength of insonating wave • range position). The speed of sound used for the AGAR was 1490 m/s and 1469 m/s for the TEM.

The 2-D image of the PSF for the LPAT was constructed from a series of azimuthal lines obtained from consecutive B-scan images, taken at the depth containing the maximum brightness from the point scatterer. (Figure 2) A study was undertaken to verify that image intensity exhibited a linear relation with ultrasound intensity. (Figure 3) The Acuson was adjusted for 0dB transmit power, 50dB log compression, 0 persistence, a linear processing curve and the gain adjusted so that the maximum reflected signal from the point scatterer produced a maximum brightness level. The TGC controls were set to the NSDG mode. The slope (S) was set to 3.5 dB/cm for the TEM target and 0 dB/cm for the AGAR target. The azimuthal data was interpolated to form the 2-D PSF image. Theoretical plots based on a simple rectangular aperture were plotted along with the cross-sectional data along the azimuthal and elevational axes.

Results

PSF of Linear Phased Array in Non-scattering Medium: Measured & Theoretical

2-D Image of PSF(Figure 4)

The data was normalized to a 0 dB maximum and plotted with a 50 dB dynamic range of intensity as indicated in the color legend. Demarcations on the axes correspond to 1mm increments.

Cross-sectional Graphs of PSF taken at intersection of PSF maximum along the azimuthal (x) and elevational (y) axes

azimuthal (x) axis (Figure 5)

elevational (y) axis (Figure 6)

PSF of Linear Phased Array in Scattering Medium: Measured & Theoretical

2-D Image of PSF(Figure 7)

The data was normalized to a 0 dB maximum and plotted with a 50 dB dynamic range of intensity as indicated in the color legend. Demarcations on the axes correspond to 1mm increments.

Cross-sectional Graph of PSF taken at intersection of PSF maximum along the azimuthal (x) and elevational (y) axes

azimuthal (x) axis (Figure 8)

elevational (y) axis (Figure 9)

Observations & Conclusions relative to Linear Phased Array

As expected, the spatial resolution in the azimuthal direction was considerably better than in the elevational direction. This can lead to significant out of plane artifacts in conventional B-scan images.

Doublet Lens

Description of Experiment

Both targets were held in position with a 3-axis adjustable mechanism such that the 0.5mm tungsten carbide sphere serving as the scattering source was 200mm (on the range axis) from the front surface of the object side of the doublet lens. A one-half inch diameter, flat, unfocused, single element transducer was located to the side of the doublet lens and aimed such that its beam axis was coplanar with the doublet lens and intersected with the beam pattern of the doublet lens at the location of the point scatterer. (Figures 10 and 11) For the AGAR target, the axis of the cylinder was aligned with the receive beam pattern of the doublet lens and oriented so that the point scatterer was 40mm behind the circular surface closest to the lens. For the TEM target, the cube was aligned so that the point scatterer was 31mm behind the surface that was perpendicular to the axis of the receive beam pattern.

From a theoretical point of view, the doublet lens can be considered as a circular aperture, to a rough approximation. Therefore, the beam intensity pattern at the imaging plane can be modeled by what is commonly referred to as a "Jinc squared" function where a "Jinc" function is given as $(J_1(r)/r)$, $J_1(\ )$ representing a Bessel function of the first kind. In this case r equals $(k \bullet l \bullet r_0) / (2 \bullet z)$ where l represents the diameter of the aperture, r_0 represents the radial distance from the range axis in the imaging plane, z represents the distance along the range axis from the aperture and k represents the wave number (frequency in radians divided by the speed of sound in the propagating medium, ω/c or $2\pi f/c$). The speed of sound used for the AGAR was 1490 m/s and 1469 m/s for the TEM.

The source of excitation was a Tektronix FNG5010 function generator running in burst mode. This provided 10 cycles of a 5 MHz sine wave. System triggering was provided by

a Tektronix PG501 pulse generator running at 5 kHz. The excitation source drove an Amplifier Research 1000 RF amplifier which was directly coupled to the 0.5" diameter flat transmit transducer.

Pressure in the imaging focal plane was obtained by scans carried out with the NTR AIMS Acoustic Intensity Measurement System. A NP-1000 0.5mm diameter hydrophone was scanned by a high-precision three dimensional positioning system under computer control. The hydrophone output was connected to a HP2130 30dB pre-amplifier. The output of the pre-amplifier was fed into a TTE KG-4 passive 5 MHz bandpass filter to reduce noise. The filtered signal was connected to the receiver of a Panametrics 5072PR pulser/receiver whose output was connected to the 50 MHz digitizer of the AIMS system for data acquisition, analysis and storage. Planar scans at the focal depth of 60mm from the center of the surface of imaging side of the doublet lens as well as line scans along the azimuthal and elevational axes were recorded for the AGAR and the TEM targets. Theoretical plots based on a simple circular aperture were plotted along with the cross-sectional data along the azimuthal and elevational axes.

Results

PSF of Doublet Lens in Non-scattering Medium: Measured & Theoretical

2-D Image of PSF(Figure 12)

The data was normalized to a 0 dB maximum and plotted with a 50 dB dynamic range of intensity as indicated in the color legend. Demarcations on the axes correspond to 1mm increments.

Cross-sectional Graphs of PSF taken at intersection of PSF maximum along the azimuthal (x) and elevational (y) axes

azimuthal (x) axis (Figure 13)

elevational (y) axis (Figure 14)

PSF of Doublet Lens in Scattering Medium: Measured & Theoretical

2-D Image of PSF(Figure 15)

The data was normalized to a 0 dB maximum and plotted with a 50 dB dynamic range of intensity as indicated in the color legend. Demarcations on the axes correspond to 1mm increments.

Cross-sectional Graph of PSF taken at intersection of PSF maximum along the azimuthal (x) and elevational (y) axes

azimuthal (x) axis (Figure 16)

elevational (y) axis (Figure 17)

Observations & Conclusions relative to Doublet Lens

As expected, the doublet lens exhibited uniform spatial resolution in both the azimuthal and elevational directions. The voltage levels outside the main lobe fell within the noise level of the measurement system. The effect of the scattering material on the PSF was to lower ratio of the main lobe signal from the point scatterer to that of the signal noise through attenuation of the transmitted pressure wave insonating the scatterer and further attenuation of the scattered pressure wave from the point scatterer. It was determined that for the linear, unfocused insonation of the target, an increase in the signal to noise ratio would require a measurement system with a lower noise floor than the experimental setup was able to provide.

Comparison of Phased Array & Doublet Lens PSF Results

PSF of Linear Phased Array & Doublet Lens in Non-scattering Medium: Measured

2-D Image of PSF(Figure 18)

The data was normalized to a 0 dB maximum and plotted with a 50 dB dynamic range of intensity as indicated in the color legend. Demarcations on the axes correspond to 1mm increments.

Cross-sectional Graph of PSF taken at intersection of PSF maximum along the azimuthal (x) and elevational (y) axes

azimuthal (x) axis (Figure 19)

elevational (y) axis (Figure 20)

PSF of Linear Phased Array & Doublet Lens in Scattering Medium: Measured

2-D Image of PSF(Figure 21)

The data was normalized to a 0 dB maximum and plotted with a 50 dB dynamic range of intensity as indicated in the color legend. Demarcations on the axes corresponds to 1mm increments.

Cross-sectional Graph of PSF taken at intersection of PSF maximum along the azimuthal (x) and elevational (y) axes

azimuthal (x) axis (Figure 22)

elevational (y) axis (Figure 23)

Observations & Conclusions regarding comparison of Doublet Lens and Linear Phased Array Transducer

An advantage of a circular aperture is that it provides uniform radial spatial resolution in the plane defined by the azimuthal and elevational axes whereas the ratio of spatial resolution of a rectangular aperture in the azimuthal and elevational direction will depend on the ratio of azimuthal and elevational dimensions of the aperture in an inverse manner.

It was demonstrated that the scattering material produced a marked improvement in the spatial resolution of the LPAT in both the azimuthal and elevational directions. Undoubtedly, commercial ultrasound imaging systems are designed for propagation in weakly scattering media such as tissue and their focusing designs for both transmit and receive are optimized for this situation. The main effect of the scattering material on the doublet lens PSF was to lower the signal to noise ratio (SNR), primarily due to the attenuation of the overall scattered signal arising from the point scatterer. A similar reduction in the SNR is also evident for the PSF of the LPAT in the scattering material. The SNR of the LPAT PSF was higher than that of the doublet lens for both the AGAR and TEM target. Two of the factors accounting for this difference are 1) lower noise floor and wider dynamic range typically found in commercial ultrasound imaging systems (typically 50 dB or greater) compared to the AIMS measurement system (approximately 35 dB of effective dynamic range when noise floor is accounted for) and 2) focused transmit pressure waves (fixed elevationally, electronically focused azimuthally) in commercial ultrasound imaging systems versus a relatively small aperture unfocused transducer in the measurement system.

Figure to be supplied at later date

Figure 1. The transducer was held in mechanical positioning system that allowed it to be scanned across the surface of the target material in precise 1mm increments in the elevation direction

Figure to be supplied at later date

Figure 2. 2D Image of the PSF for the LPAT constructed from a series of azimuthal lines obtained from consecutive B-scan images, taken at the depth containing the maximum brightness from the point scatterer.

(Figure 3)

Video Density Calibration of Acuson 128/XP

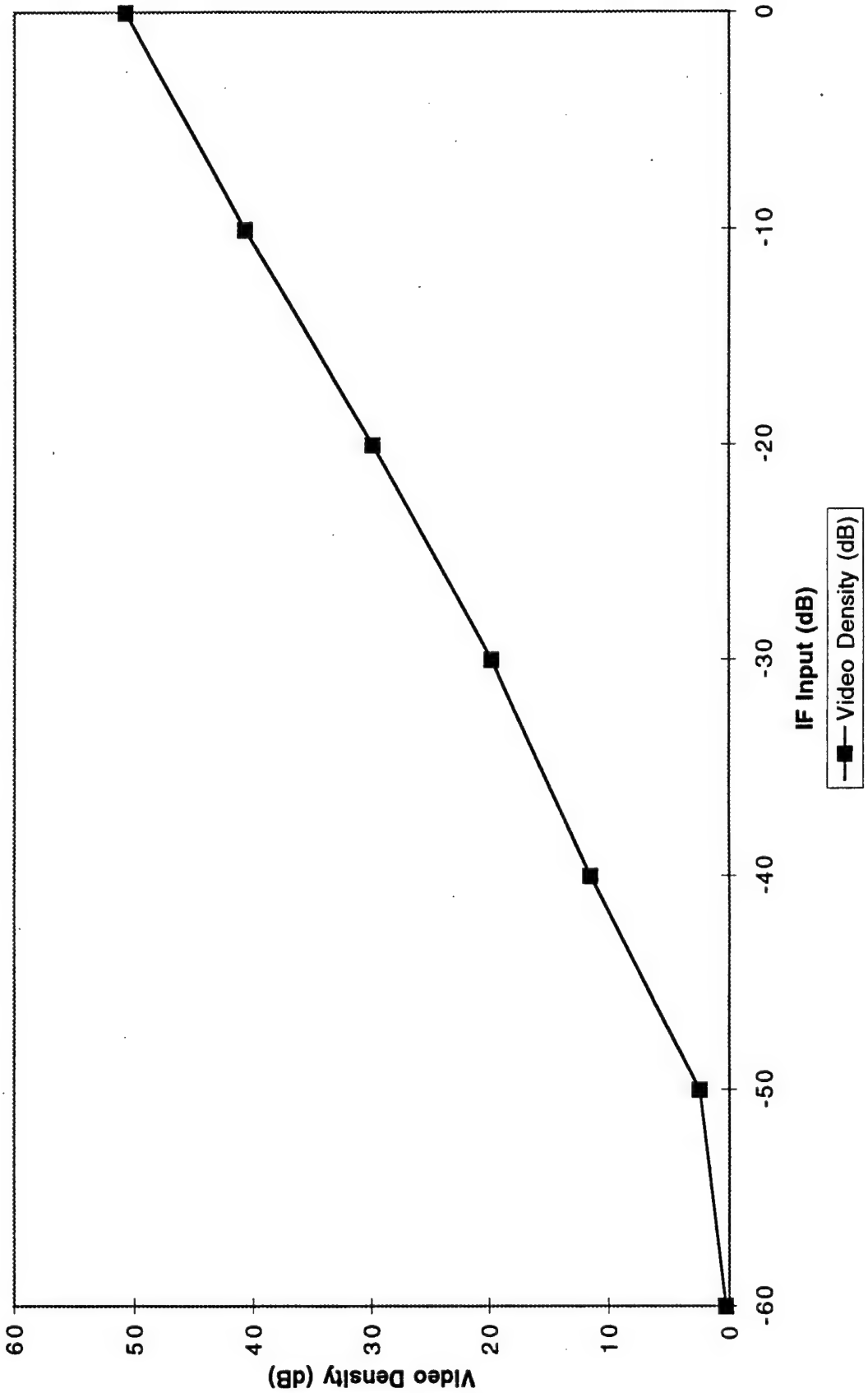

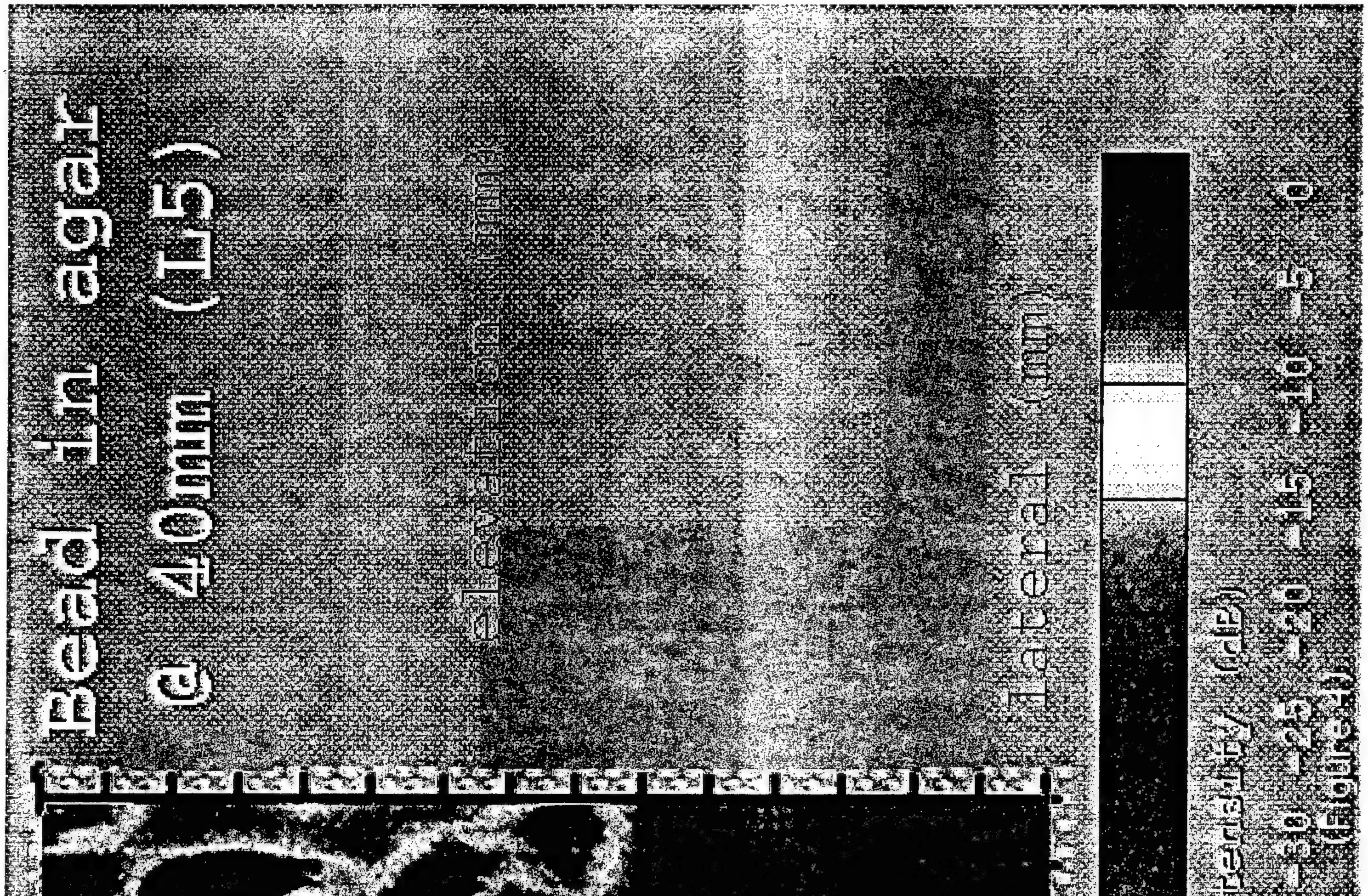
Bead in agar
@ 40mm (L5)
elevation (mm)
lateral (mm)
Intensity (dB)
-50 -45 -40 -35 -30 -25 -20 -15 -10 -5 0
(figure 4)

(Figure 5)

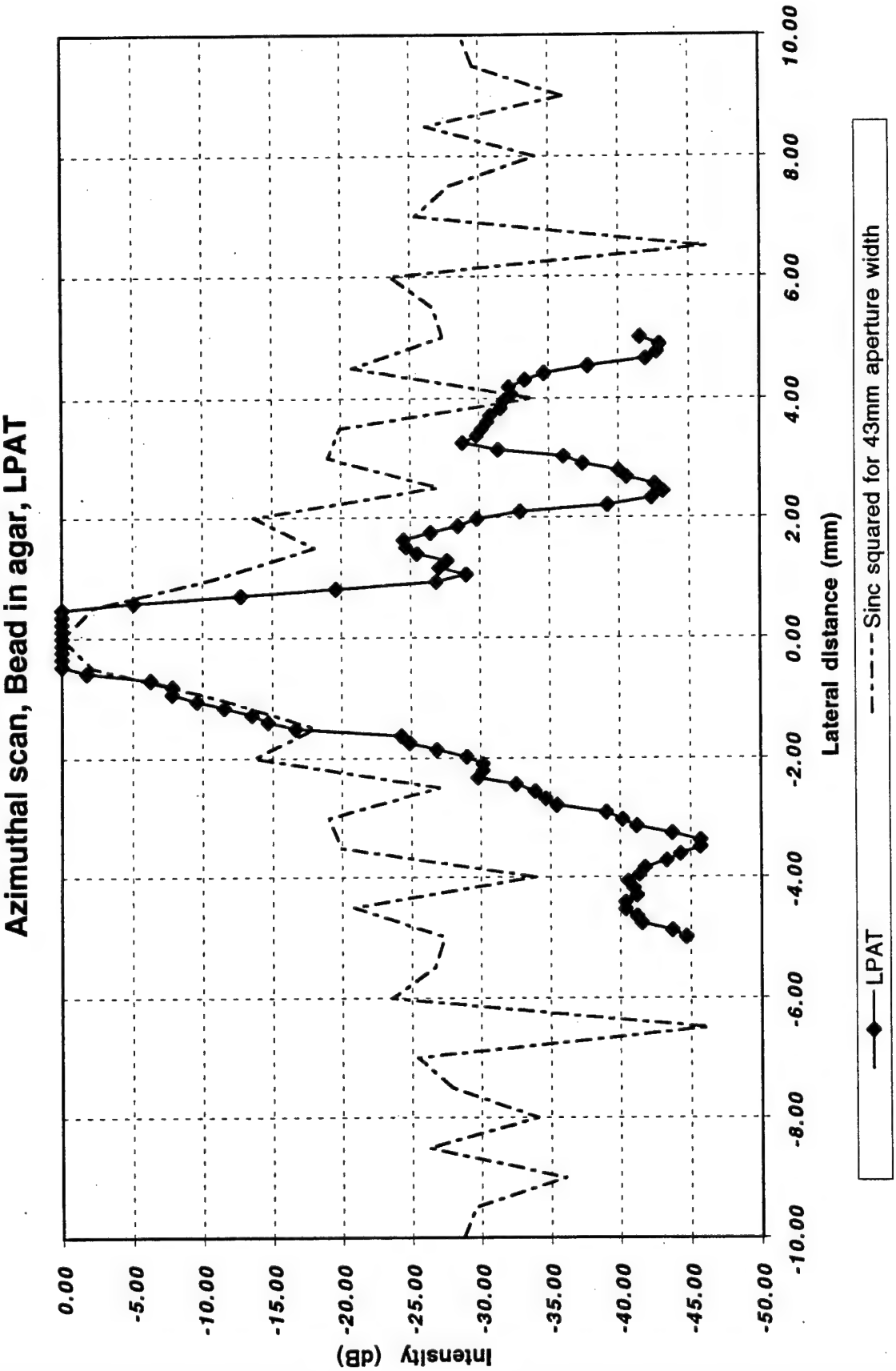
Azimuthal scan, Bead in agar, LPAT
Intensity (dB)
0.00
-5.00
-10.00
-15.00
-20.00
-25.00
-30.00
-35.00
-40.00
-45.00
-50.00
-10.00
-8.00
-6.00
-4.00
-2.00
0.00
2.00
4.00
6.00
8.00
10.00
Lateral distance (mm)
LPAT
Sinc squared for 43mm aperture width

(Figure 6)

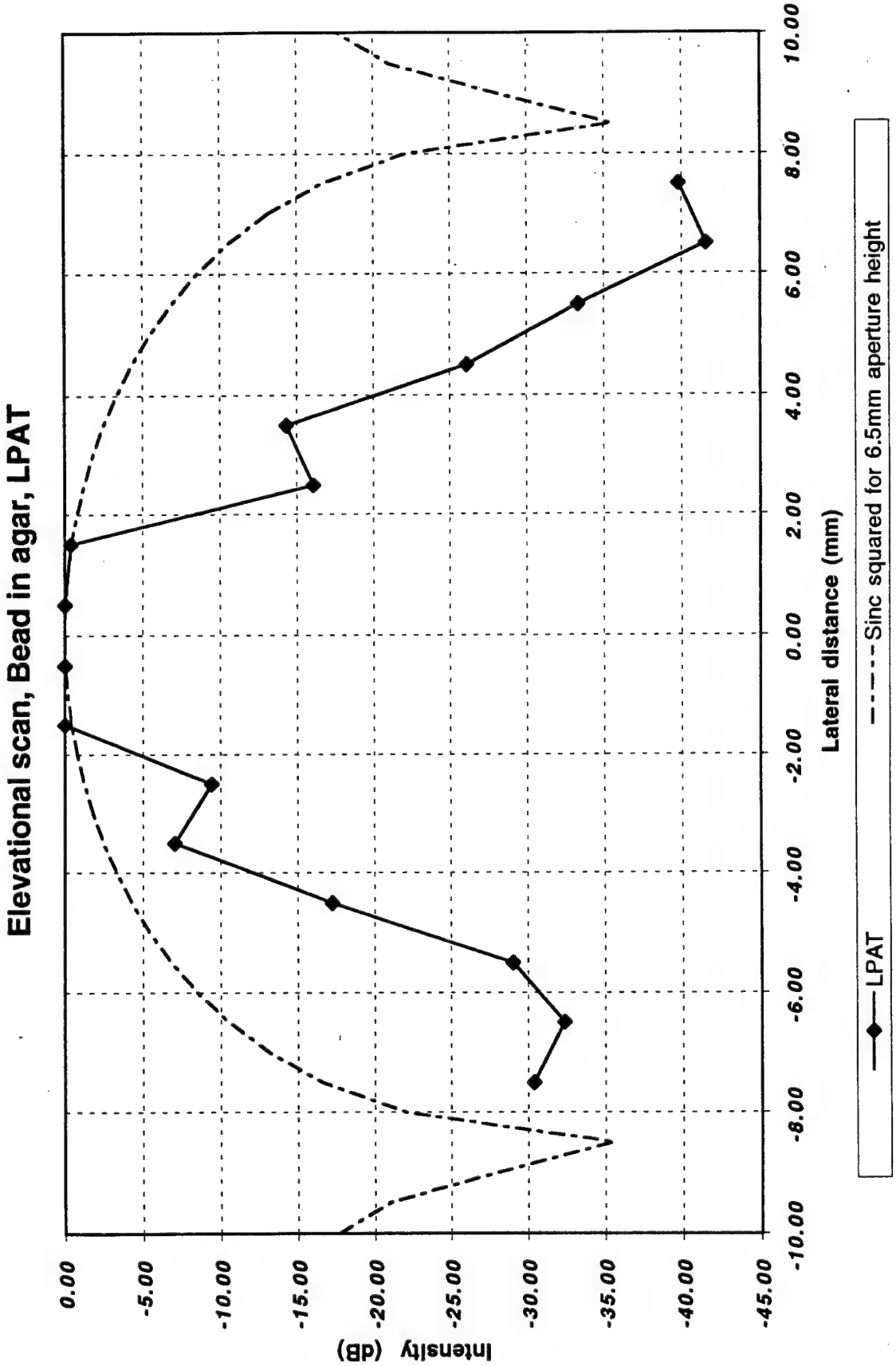
Elevational scan, Bead in agar, LPAT
Intensity (dB)
0.00
-5.00
-10.00
-15.00
-20.00
-25.00
-30.00
-35.00
-40.00
-45.00
-10.00
-8.00
-6.00
-4.00
-2.00
0.00
2.00
4.00
6.00
8.00
10.00
Lateral distance (mm)
LPAT
Sinc squared for 6.5mm aperture height

AlN cube/bead
a 31 mm (1.5
elevation (mm)
lateral (mm)
Transmit (dB)
-50 -45 -40 -35 -30 -25 -20 -15 -10 -5 0
(relative)

(Figure 8)

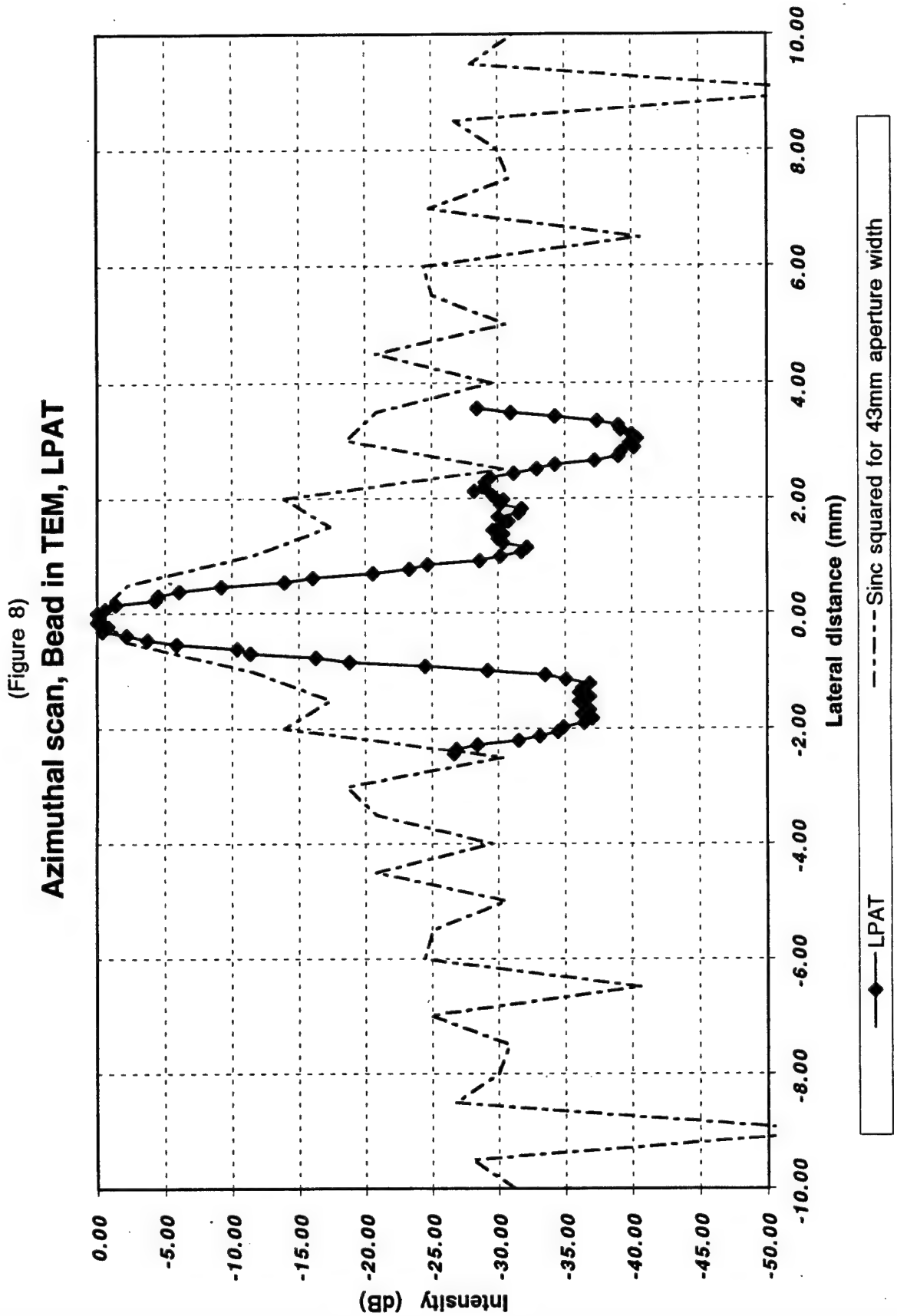
Azimuthal scan, Bead in TEM, LPAT
Intensity (dB)
0.00
-5.00
-10.00
-15.00
-20.00
-25.00
-30.00
-35.00
-40.00
-45.00
-50.00
-10.00
-8.00
-6.00
-4.00
-2.00
0.00
2.00
4.00
6.00
8.00
10.00
Lateral distance (mm)
LPAT
Sinc squared for 43mm aperture width

(Figure 9)

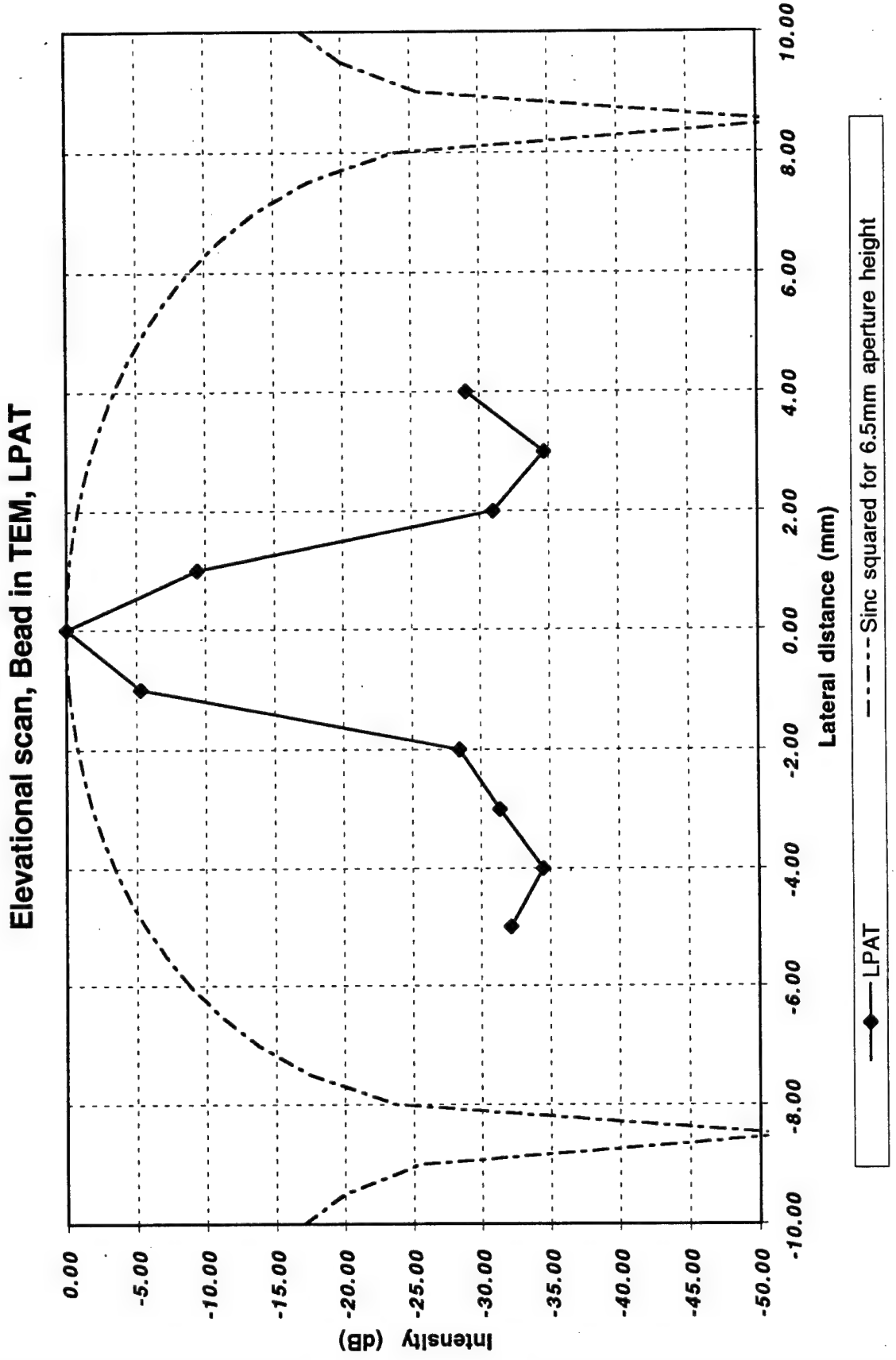
Elevational scan, Bead in TEM, LPAT
Intensity (dB)
0.00
-5.00
-10.00
-15.00
-20.00
-25.00
-30.00
-35.00
-40.00
-45.00
-50.00
Lateral distance (mm)
10.00
8.00
6.00
4.00
2.00
0.00
-2.00
-4.00
-6.00
-8.00
-10.00
LPAT
Sinc squared for 6.5mm aperture height

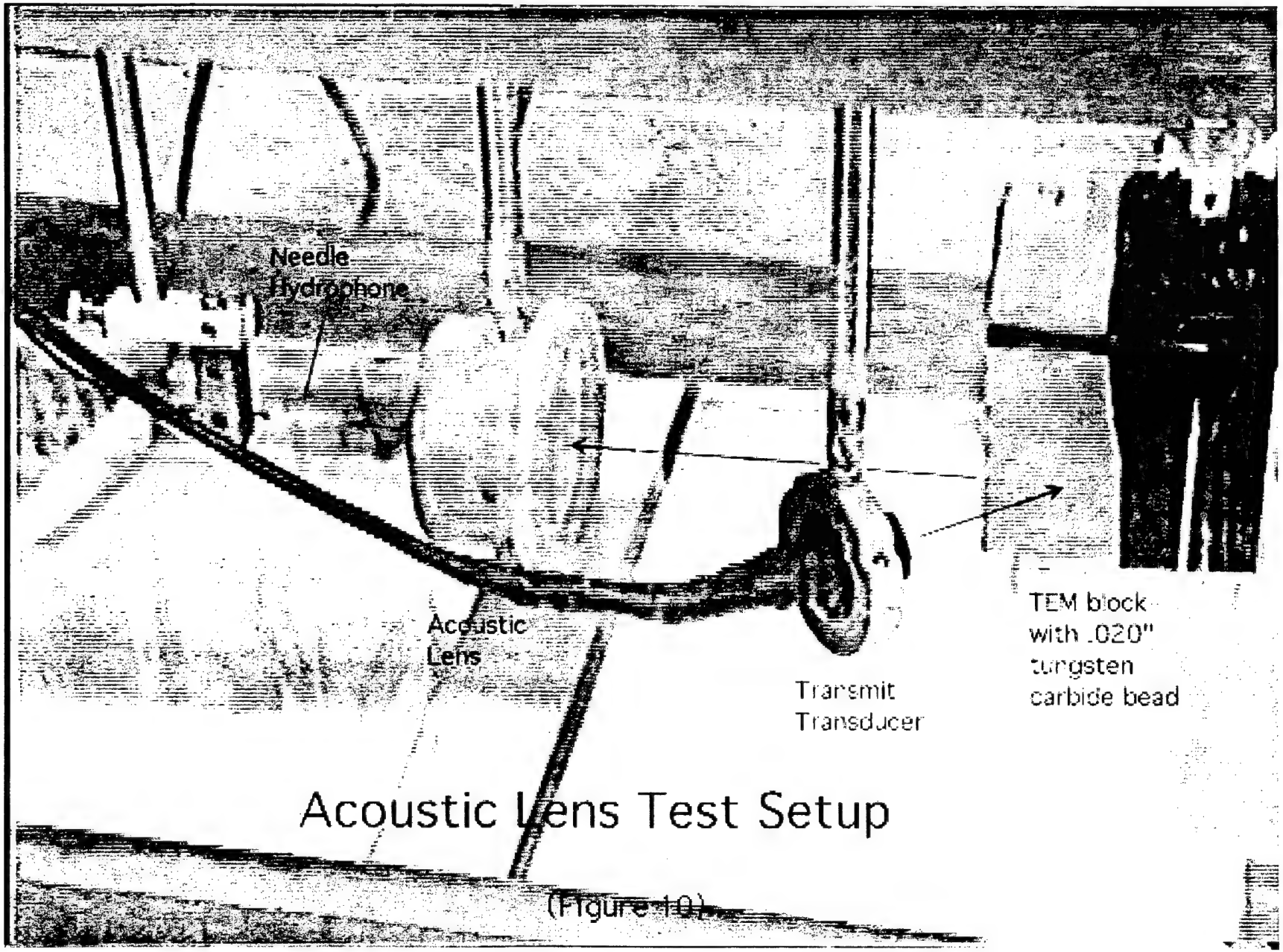

Acoustic Lens Test Setup

(Figure 10)

(Figure 11)

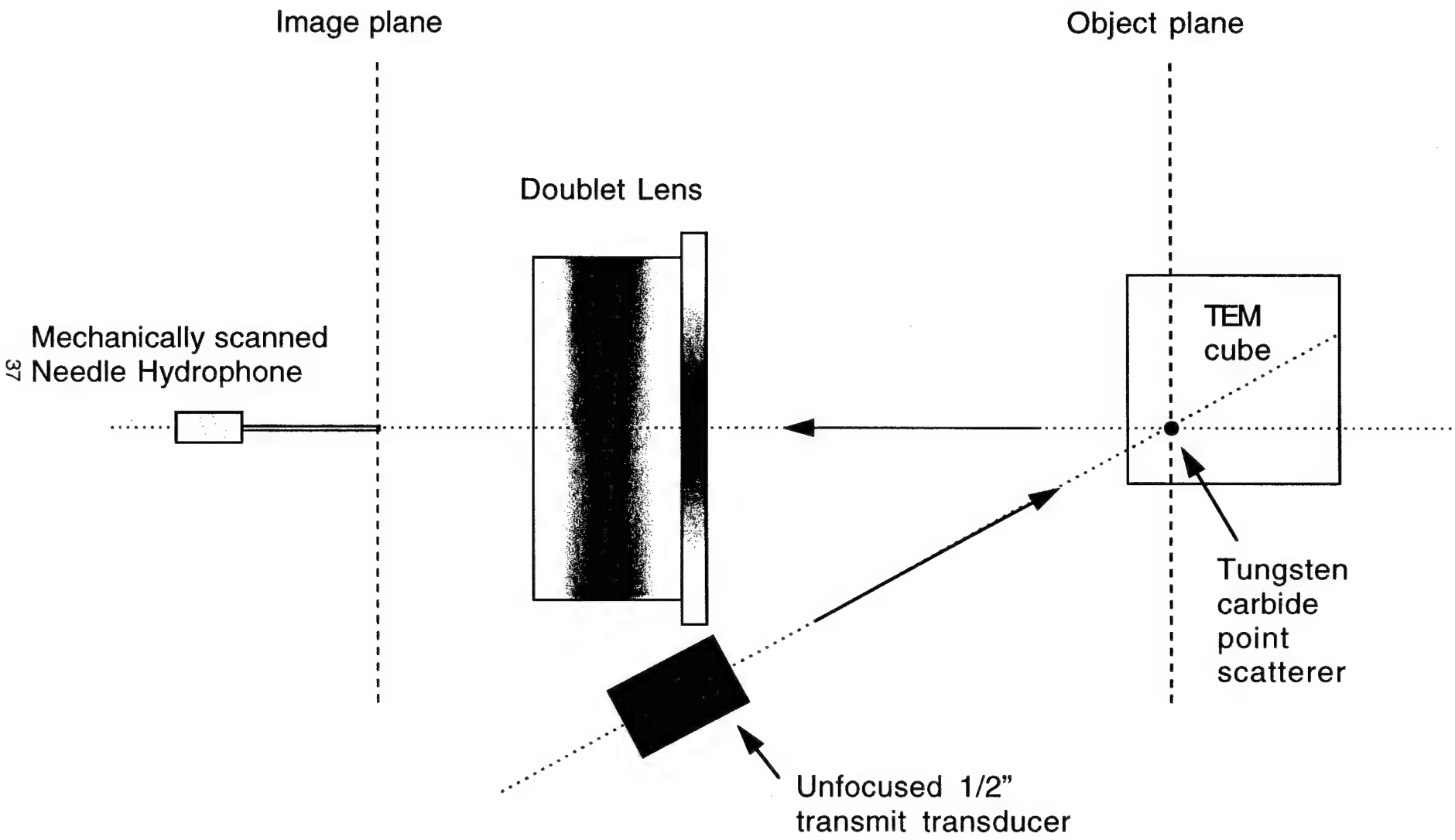
Image plane
Object plane
Doublet Lens
Mechanically scanned
Needle Hydrophone
TEM
cube
Tungsten
carbide
point
scatterer
Unfocused 1/2"
transmit transducer

Beam in aperture @ 40mm (Lens)
(Figure 12)
elevation (2mm)
azimuth (2 mm)
Intensity (dB)
0
-5
-10
-15
-20
-25
-30
-35
-40
-45
-50

(Figure 13)

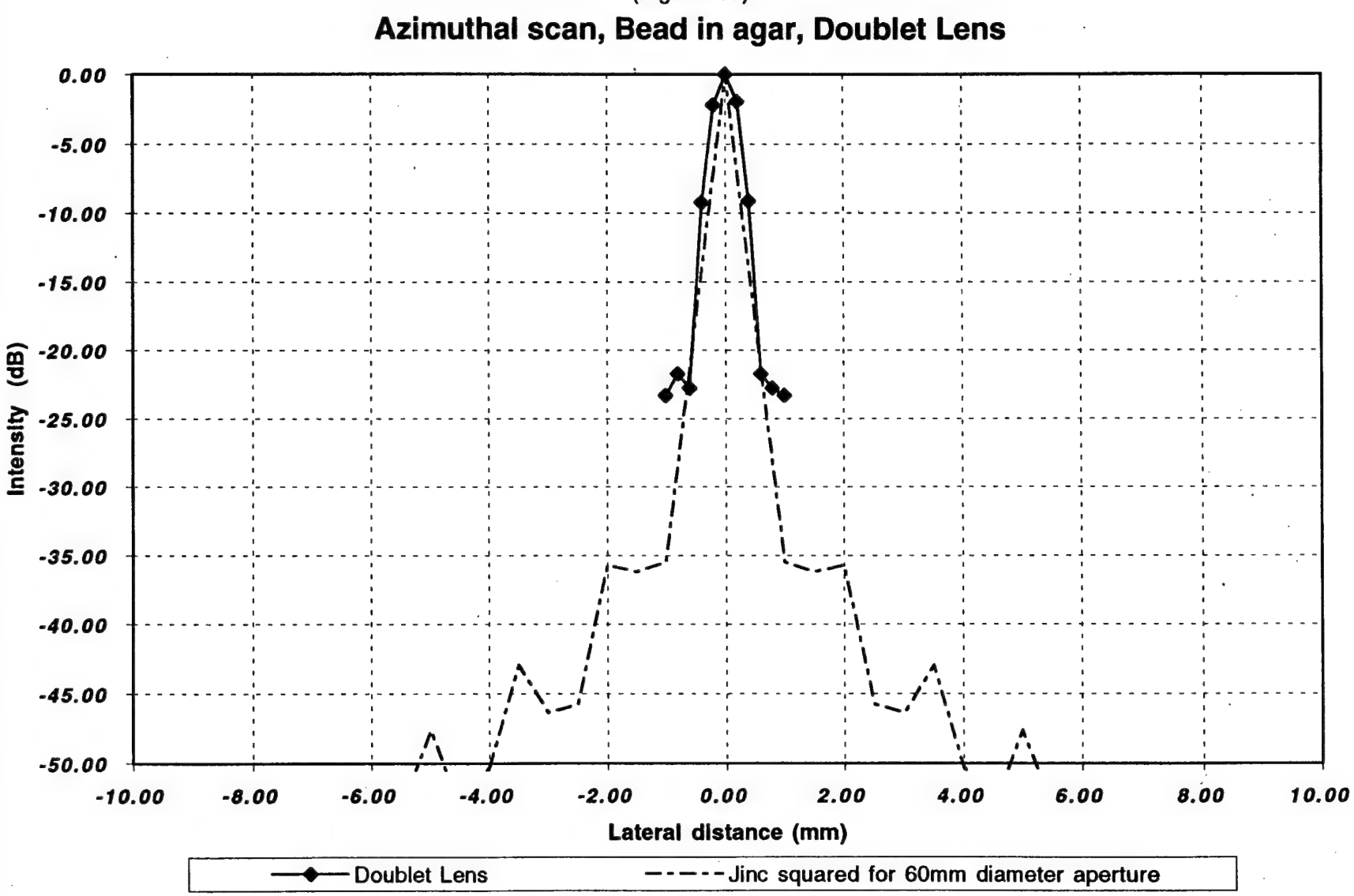
Azimuthal scan, Bead in agar, Doublet Lens
0.00
-5.00
-10.00
-15.00
-20.00
-25.00
-30.00
-35.00
-40.00
-45.00
-50.00
Intensity (dB)
-10.00
-8.00
-6.00
-4.00
-2.00
0.00
2.00
4.00
6.00
8.00
10.00
Lateral distance (mm)
Doublet Lens
Jinc squared for 60mm diameter aperture

(Figure 14)

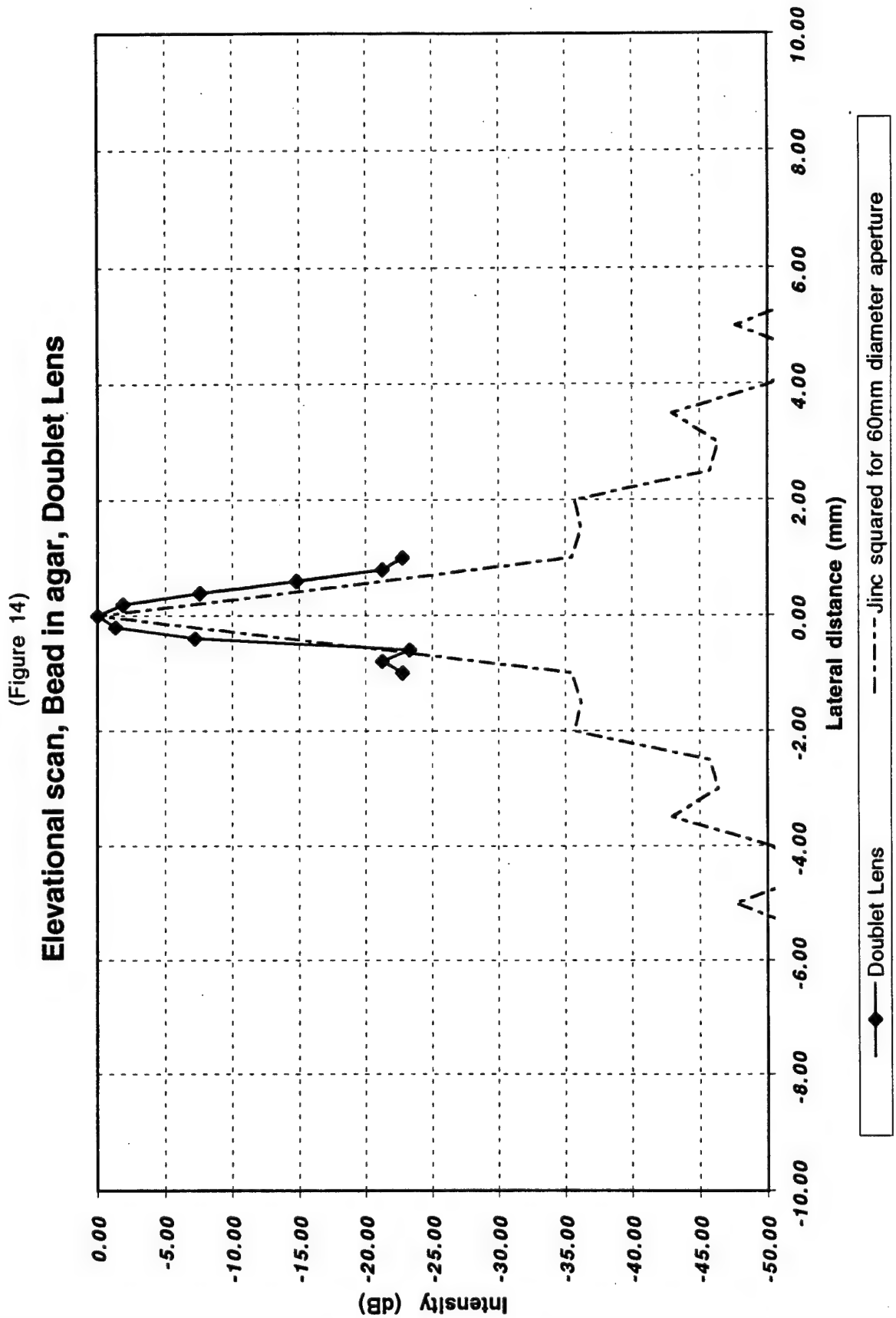
Elevational scan, Bead in agar, Doublet Lens
Intensity (dB)
0.00
-5.00
-10.00
-15.00
-20.00
-25.00
-30.00
-35.00
-40.00
-45.00
-50.00
10.00
8.00
6.00
4.00
2.00
0.00
-2.00
-4.00
-6.00
-8.00
-10.00
Lateral distance (mm)
Doublet Lens
Jinc squared for 60mm diameter aperture

(Figure 15)

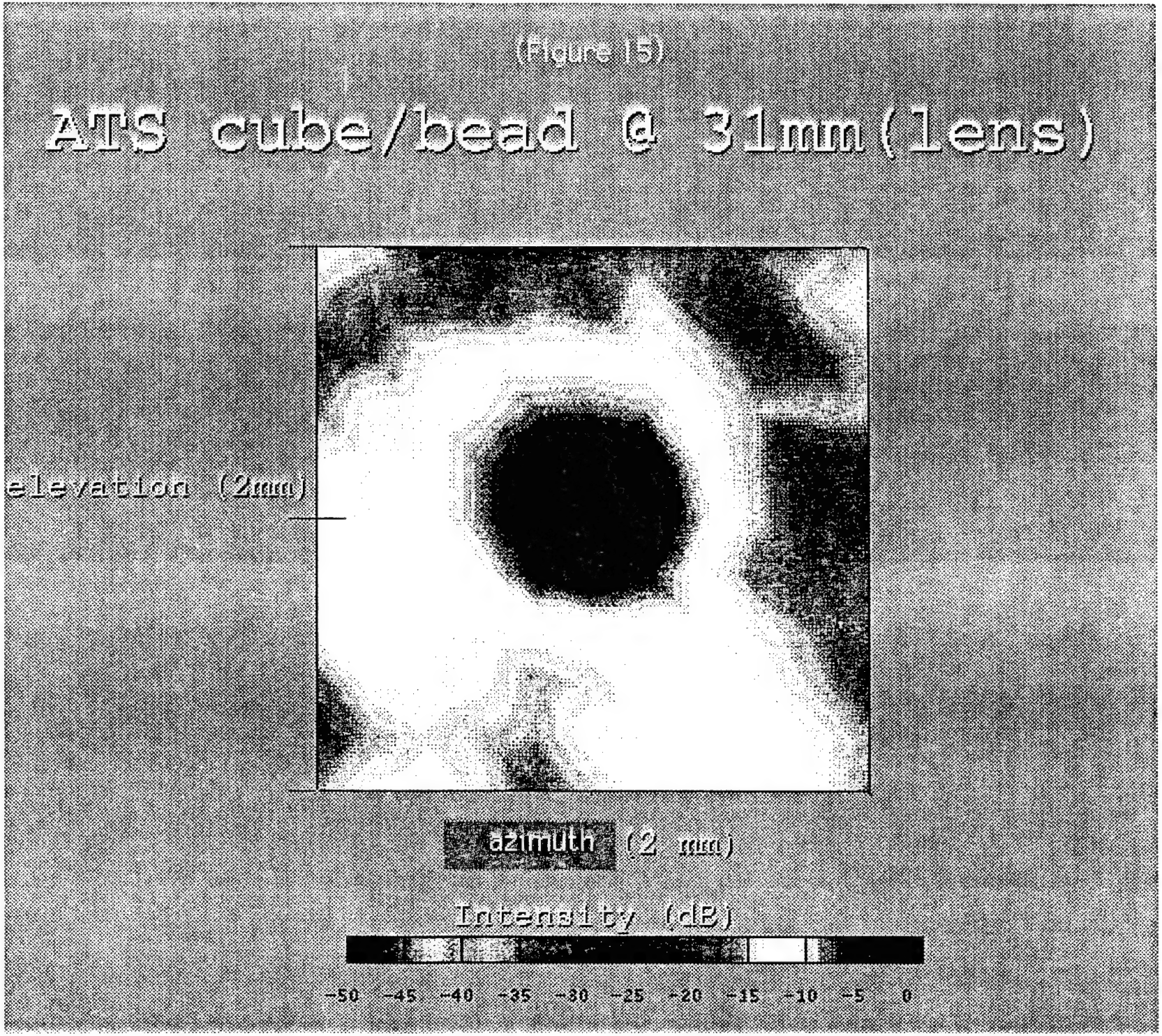
ATS cube/bead @ 31mm(lens)
elevation (2mm)
azimuth (2 mm)
Intensity (dB)
-50 -45 -40 -35 -30 -25 -20 -15 -10 -5 0

(Figure 16)

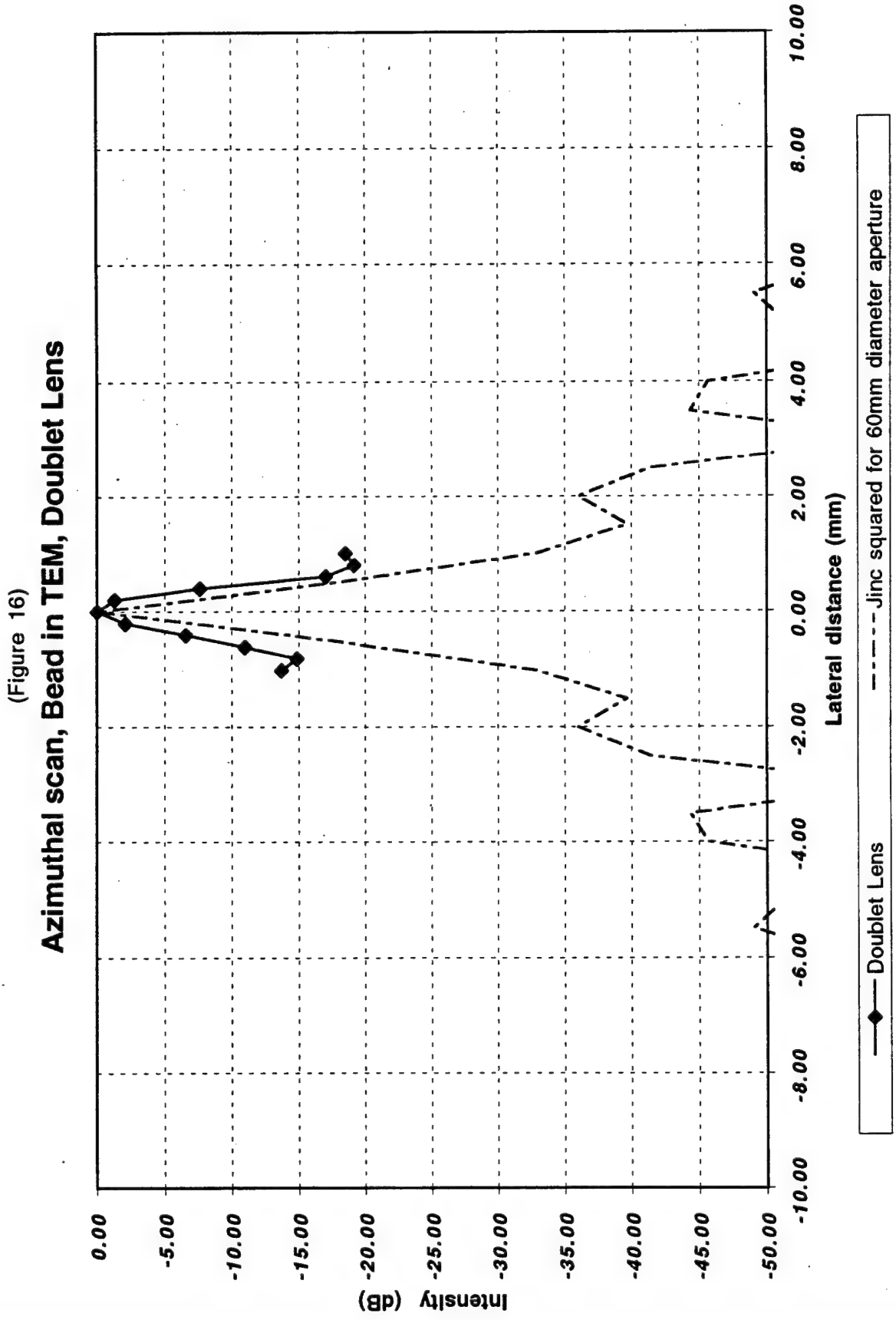
Azimuthal scan, Bead in TEM, Doublet Lens
Intensity (dB)
0.00
-5.00
-10.00
-15.00
-20.00
-25.00
-30.00
-35.00
-40.00
-45.00
-50.00
-10.00
-8.00
-6.00
-4.00
-2.00
0.00
2.00
4.00
6.00
8.00
10.00
Lateral distance (mm)
Doublet Lens
Jinc squared for 60mm diameter aperture

(Figure 17)

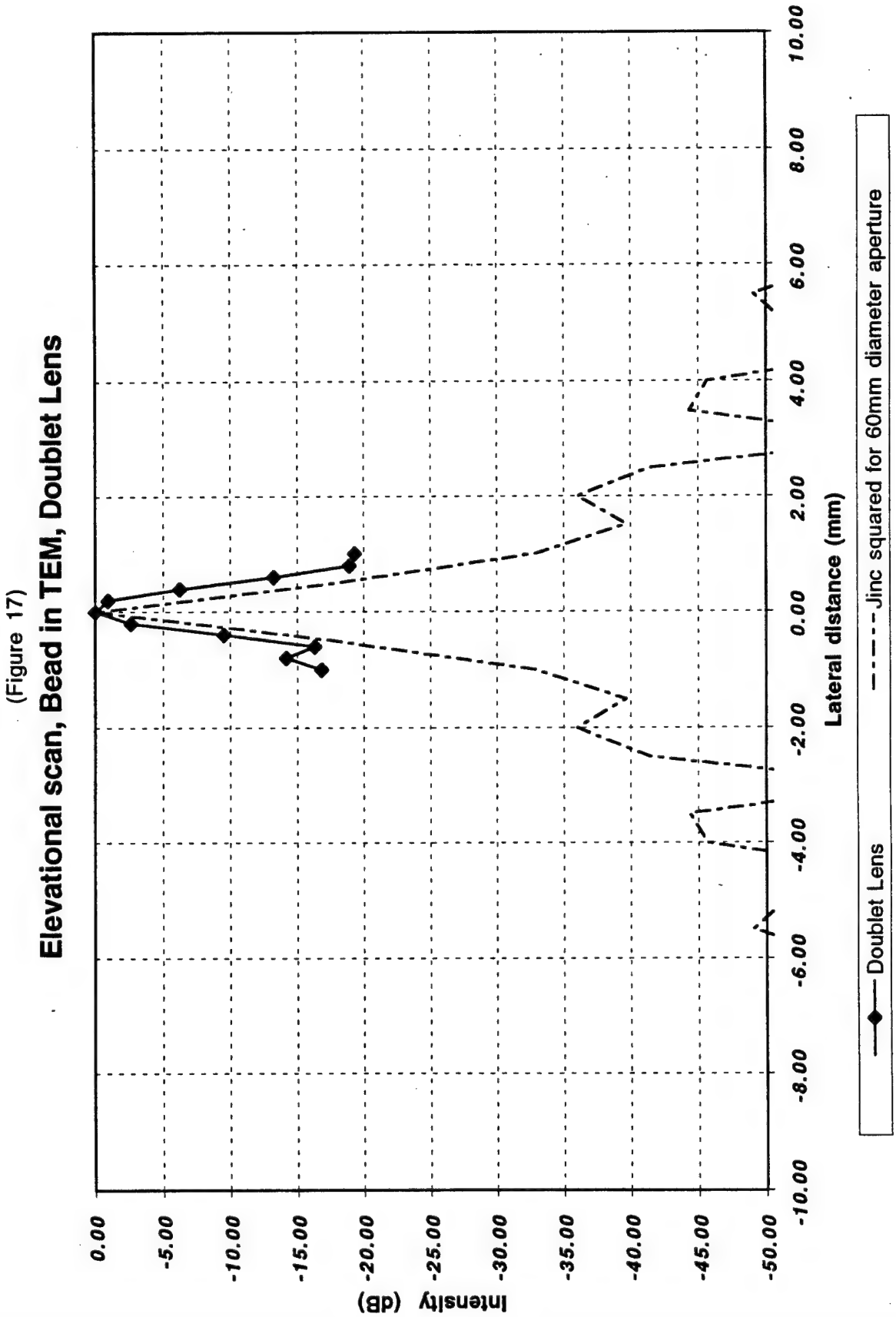
Elevational scan, Bead in TEM, Doublet Lens
Intensity (dB)
0.00
-5.00
-10.00
-15.00
-20.00
-25.00
-30.00
-35.00
-40.00
-45.00
-50.00
Lateral distance (mm)
10.00
8.00
6.00
4.00
2.00
0.00
-2.00
-4.00
-6.00
-8.00
-10.00
Doublet Lens
Jinc squared for 60mm diameter aperture

Bead in agar
@ 40mm
(T5)
(Lens)
elevation (mm)
azimuth (mm)
Intensity (dB)
-50 -45 -40 -35 -30 -25 -20 -15 -10 -5 0
(field 6)

(Figure 19)

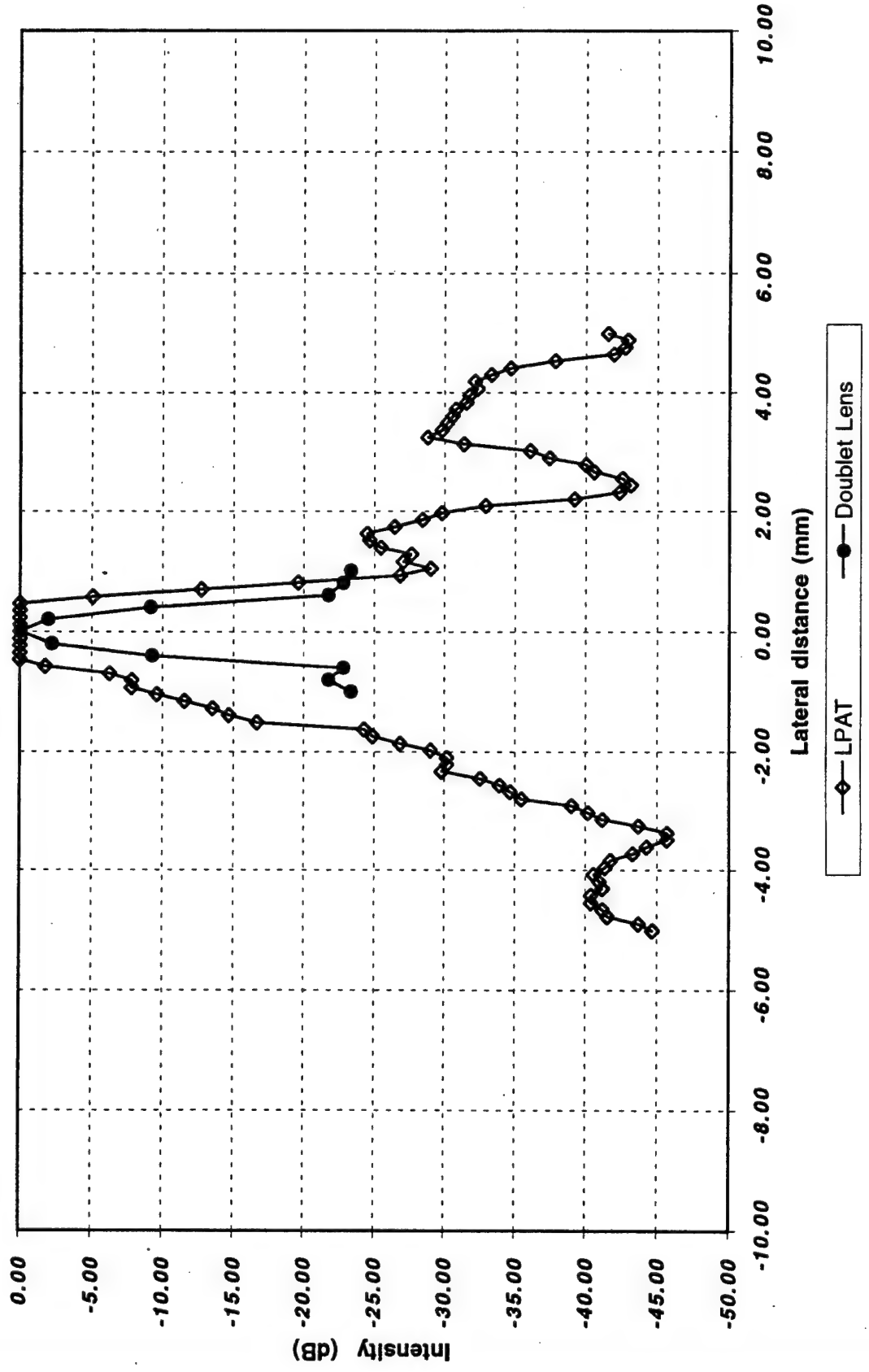
Azimuthal scan, Bead in agar, Comparison of LPAT and Doublet Lens
Intensity (dB)
0.00
-5.00
-10.00
-15.00
-20.00
-25.00
-30.00
-35.00
-40.00
-45.00
-50.00
-10.00
-8.00
-6.00
-4.00
-2.00
0.00
2.00
4.00
6.00
8.00
10.00
Lateral distance (mm)
LPAT
Doublet Lens

(Figure 20)

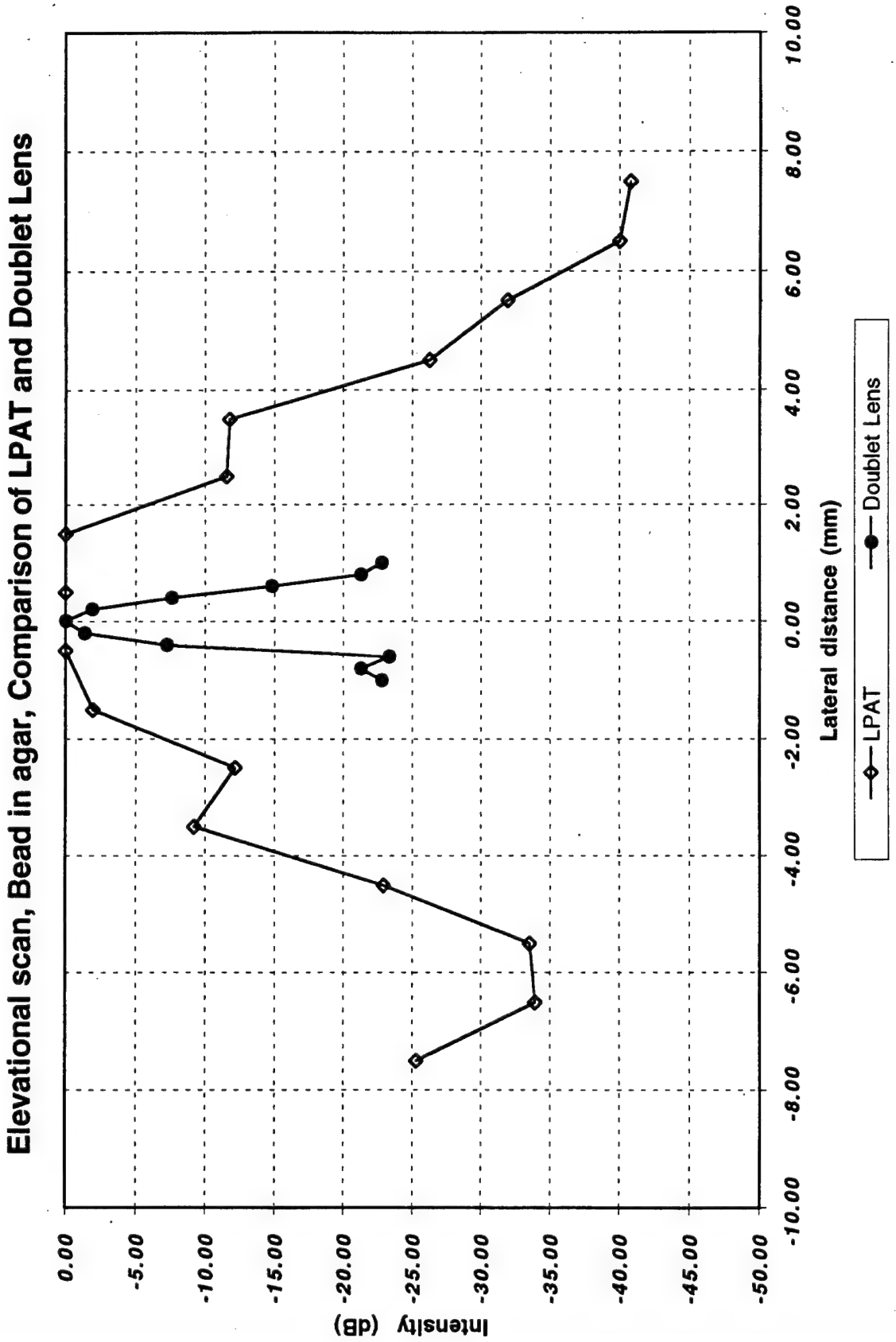
Elevational scan, Bead in agar, Comparison of LPAT and Doublet Lens
Intensity (dB)
0.00
-5.00
-10.00
-15.00
-20.00
-25.00
-30.00
-35.00
-40.00
-45.00
-50.00
Lateral distance (mm)
-10.00
-8.00
-6.00
-4.00
-2.00
0.00
2.00
4.00
6.00
8.00
10.00
LPAT
Doublet Lens

APS cube/bead
@ 31 mm
(15)
(Lens)
elevation (mm)
azimuth (mm)
Intensity (dB)
-50 -45 -40 -35 -30 -25 -20 -15 -10 -5 0
(below -25)

(Figure 22)

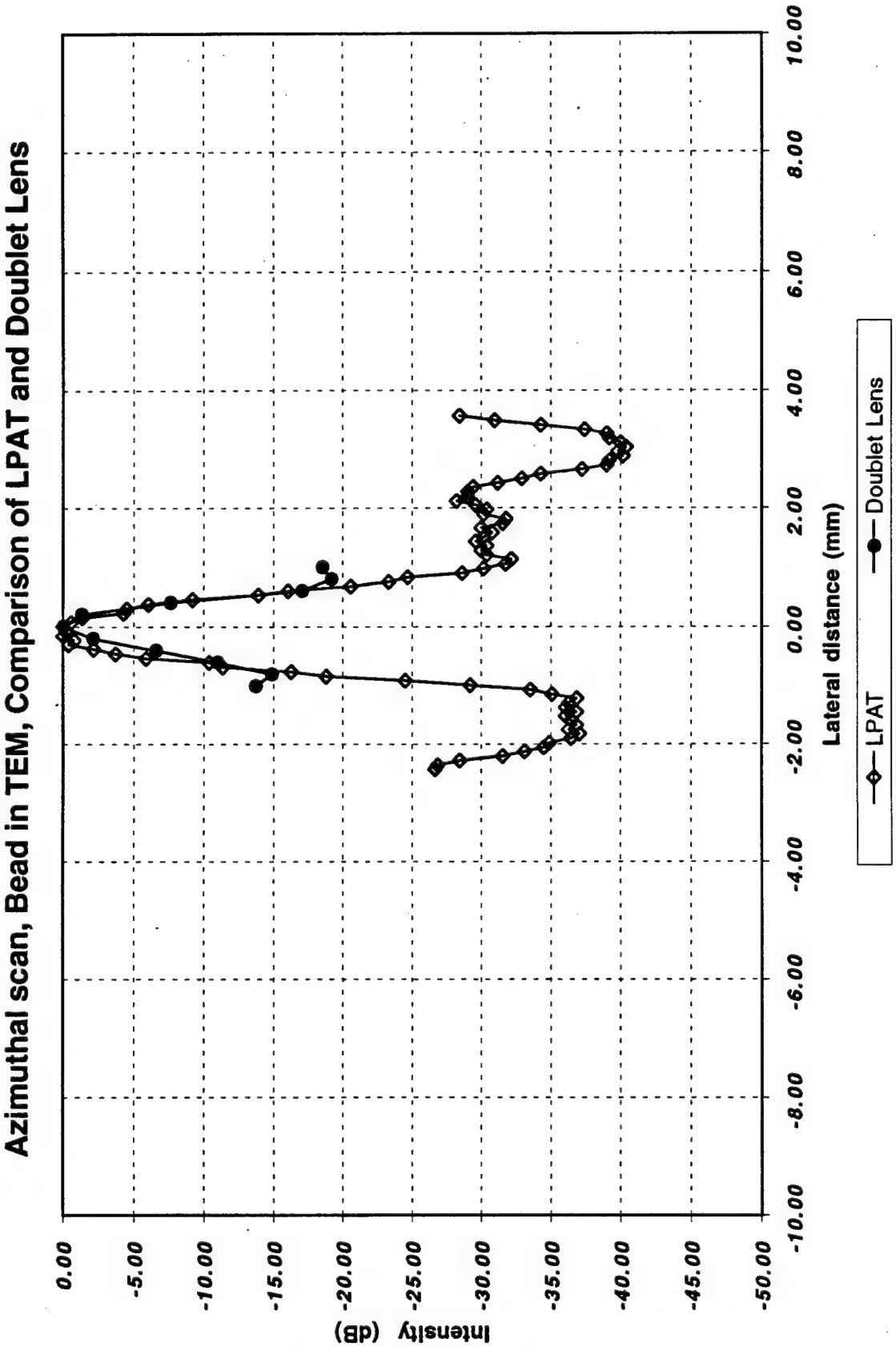
Azimuthal scan, Bead in TEM, Comparison of LPAT and Doublet Lens
Intensity (dB)
0.00
-5.00
-10.00
-15.00
-20.00
-25.00
-30.00
-35.00
-40.00
-45.00
-50.00
Lateral distance (mm)
-10.00
-8.00
-6.00
-4.00
-2.00
0.00
2.00
4.00
6.00
8.00
10.00
LPAT
Doublet Lens

(Figure 23)

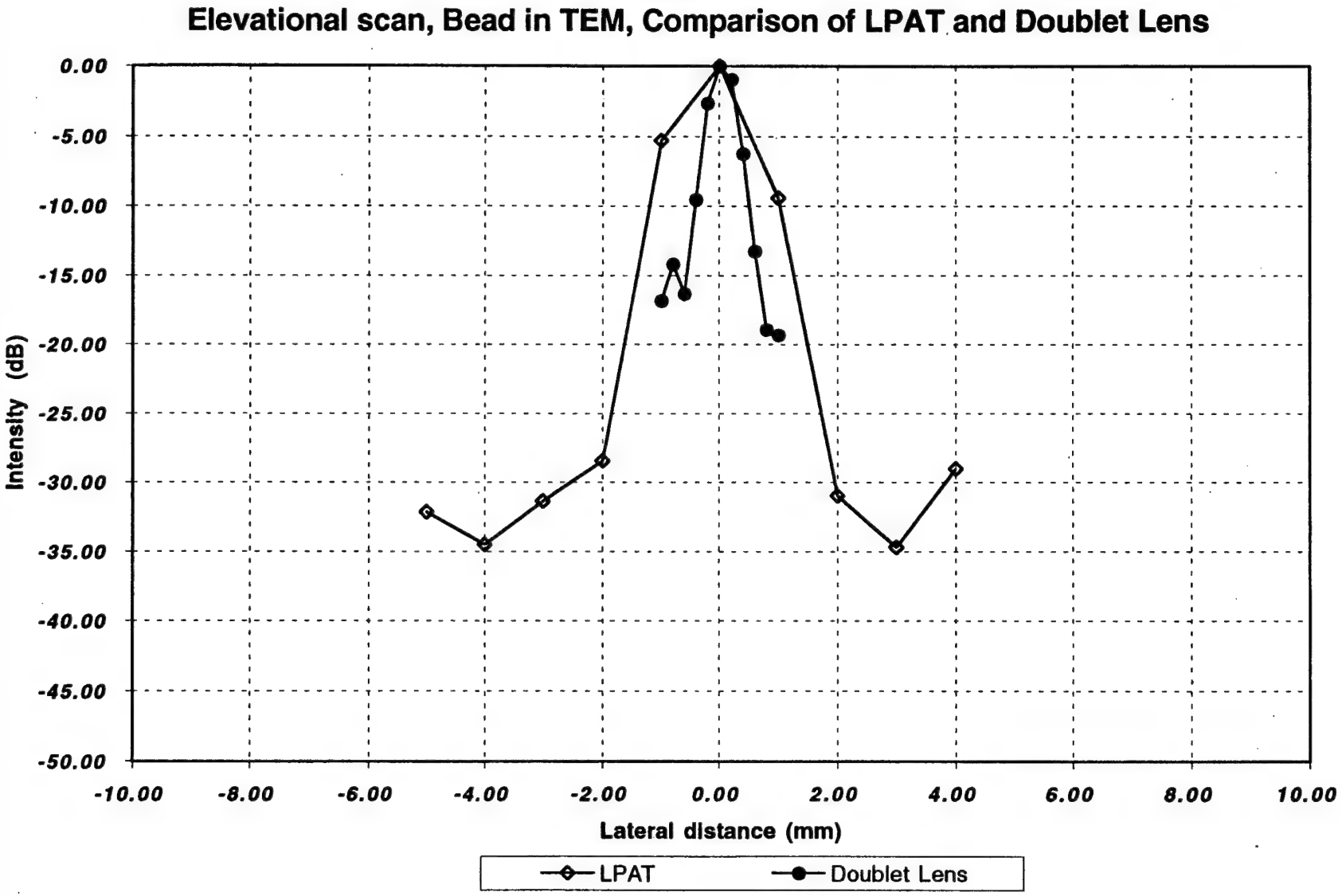
Elevational scan, Bead in TEM, Comparison of LPAT and Doublet Lens
0.00
-5.00
-10.00
-15.00
-20.00
-25.00
-30.00
-35.00
-40.00
-45.00
-50.00
Intensity (dB)
-10.00
-8.00
-6.00
-4.00
-2.00
0.00
2.00
4.00
6.00
8.00
10.00
Lateral distance (mm)
LPAT
Doublet Lens

APPENDIX A
PROBE ASSEMBLY

- Minimize Size and Weight
- Minimize Footprint on Body
- Provide Bubble Trap and Fill Port
- Minimize Electrical Power
- Non-Toxic Working Fluid
- Rugged
- Image from 0 - 15 cm Depth
- Thermally Stabilized for Patient Comfort
- Patient Interface Easily Cleaned

Figure A-1. Probe Requirements

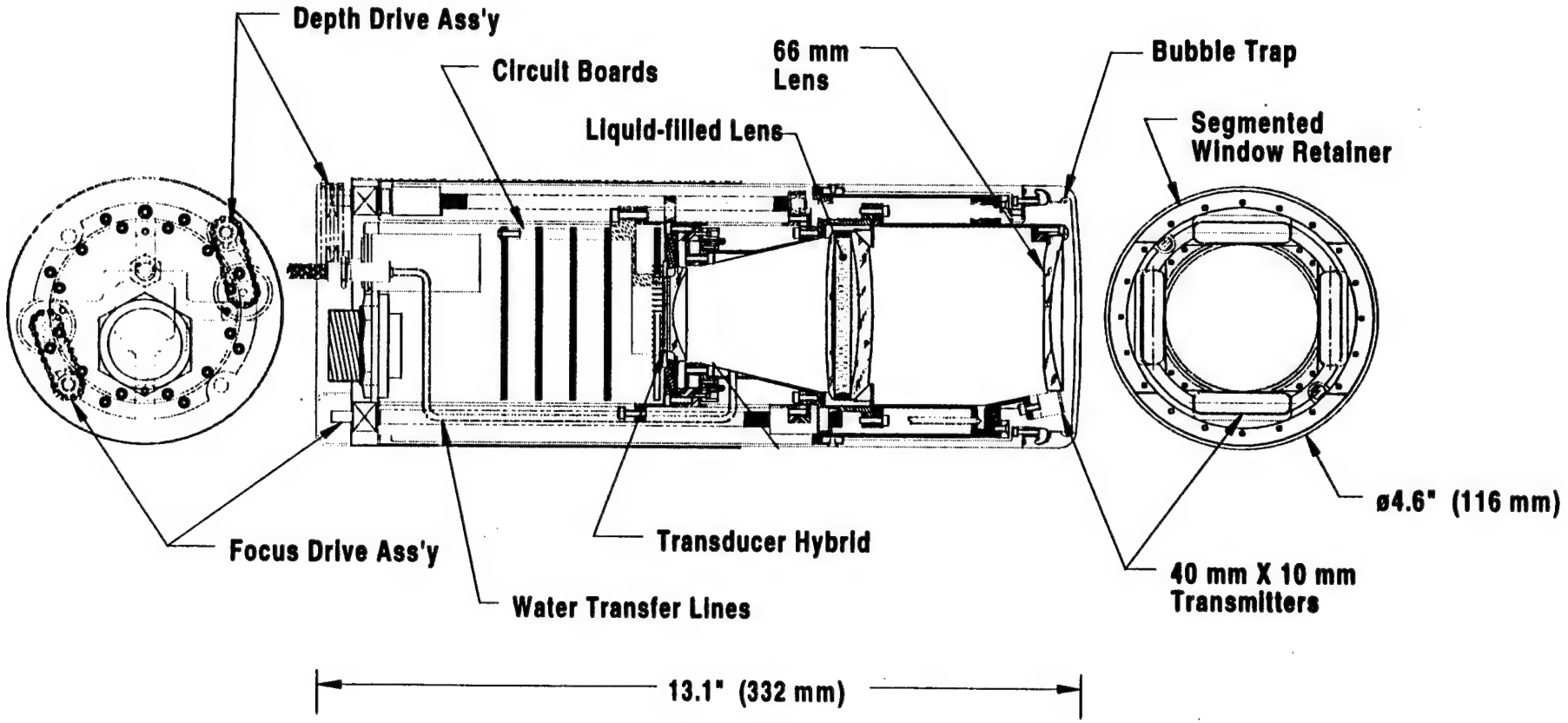

Figure A-2. BUDI Probe Configuration

Fixed Case Length

- Optics & Transducer move within constant water volume, all within Probe Ass'y.
- Probe 6" dia X 17". Contains ~ 7.5 litres (2 gallons) water.
- Lead screws operate in water with rotary seals to motors.
- Hybrid & PCB contained within sealed "Wet Box". "Wet Cable" penetrates enclosure. Multiple seals required.

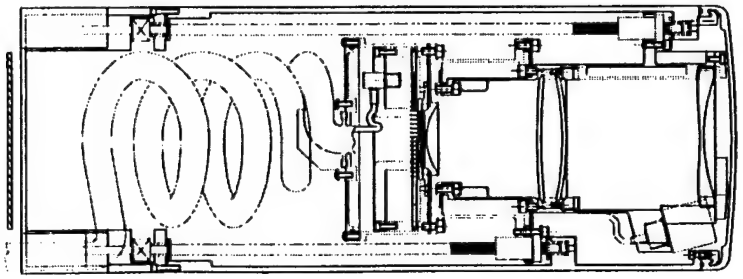

Variable Case Length

- Patient Interface Window is moved relative to Optics and Transducer.
- Water volume make-up via separate Accumulator/filtration system.
- Probe 4.6" dia X 13" min/19" max. Water volume in probe .75-2.0 litres.
- All drives and electronics outside water-filled volume.
- Rolling diaphragm seals and fewer o-ring seals required.

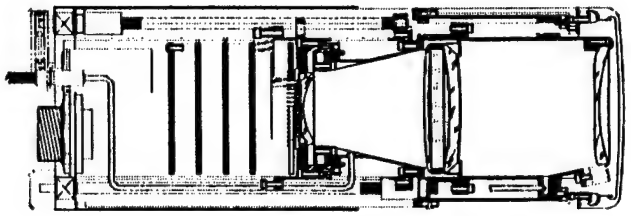

Figure A-3. Probe Configuration is Result of Design Trades

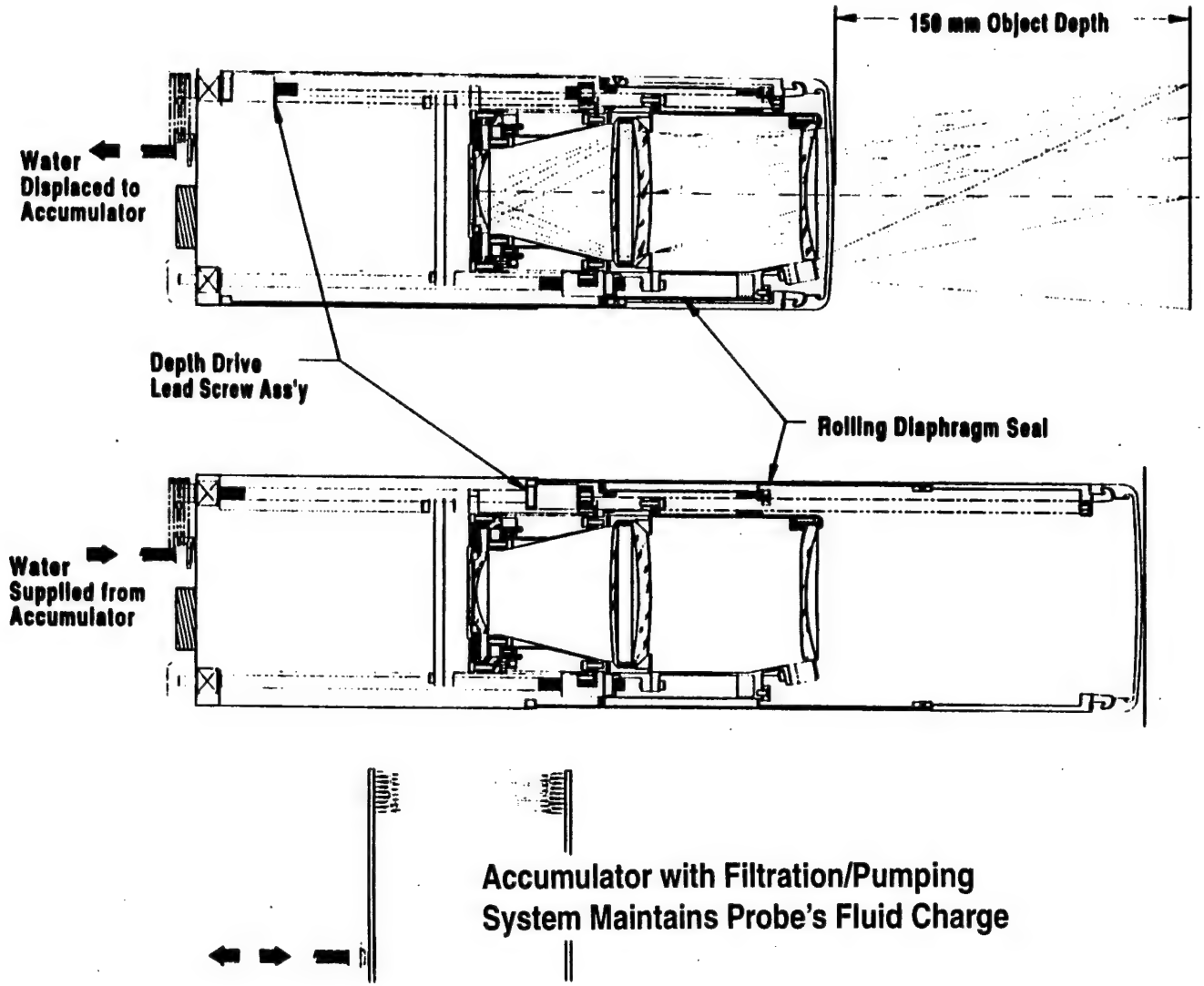

Figure A-4. Object Imaging Depth Variable Over 15+ cm Range

- **Lead Screw Ass'ys: .25" dia, .025 for both drives.**
  - Stainless Steel, rolled-thread screws with Delrin anti-backlash preloaded nuts.
  - Screws with 8 oz-in motors, encoders, and cable-chain timing drives are mounted stationary relative to Hybrid & electronics ass'y.
- **Depth Drive moves fwd outer case and window thru 15 cm.**
  - Nut is attached to flange at aft end of probe case.
  - Rolling diaphragm seal and o-ring'ed guide shafts form mechanical interface.
  - 2-speed travel control. 1 cm/sec max rate easily achieved by motor.
- **Focus Drive moves Lenses 1 & 2 thru 6 mm.**
  - Nut is attached to optics housing which carries the lenses.
  - Annular flexures provide necessary compliance in axial direction only, securely retain alignment of optics in all other directions.
  - Small secondary rolling diaphragm seal across flexure span.

Figure A-5. Depth and Focus Drives Employ Similar Hardware Solutions

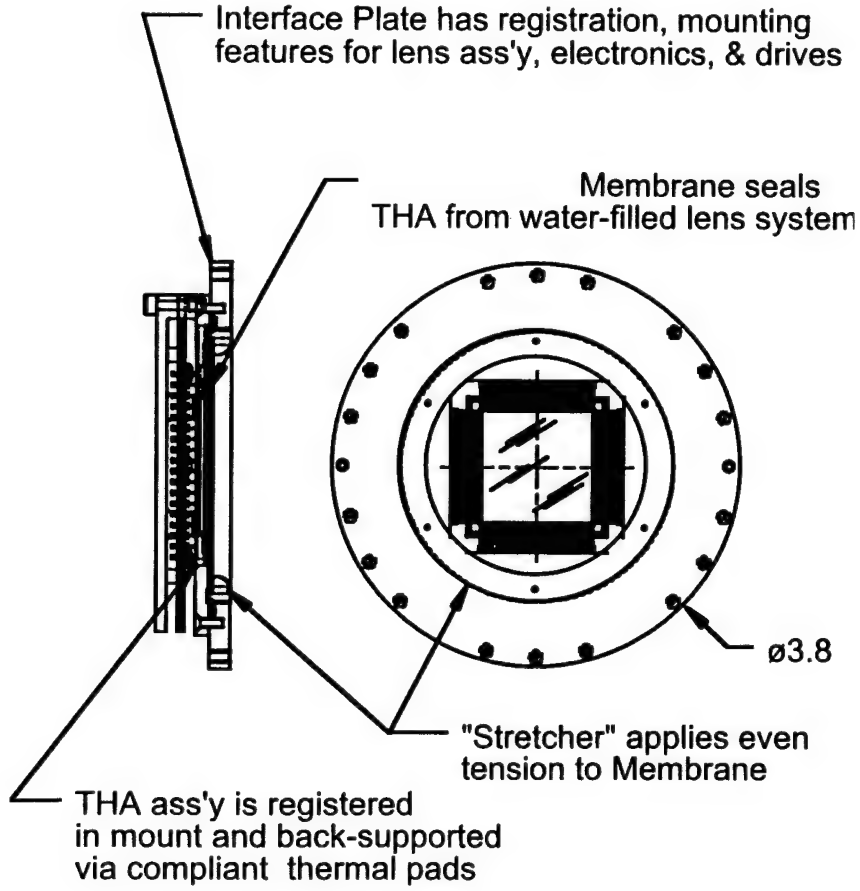

- Membrane passes sound energy from water to THA.
- Interface plate is Probe's main physical reference.
- Back Support maintains THA/PGA registration against its Mount and provides interfaces for four PCB's.
- Ass'y is stationary relative to depth and focus drives.

Figure A-6. Transducer Hybrid Interfaces to Lens Via Membrane

- **Preliminary Design Complete**
- **Prototype is Compatible with Clinical Evaluation**
- **Uses Proven Mechanical Construction Techniques**

Figure A-7. Probe Status Considerations

APPENDIX B
TRANSMITTER TRANSDUCER

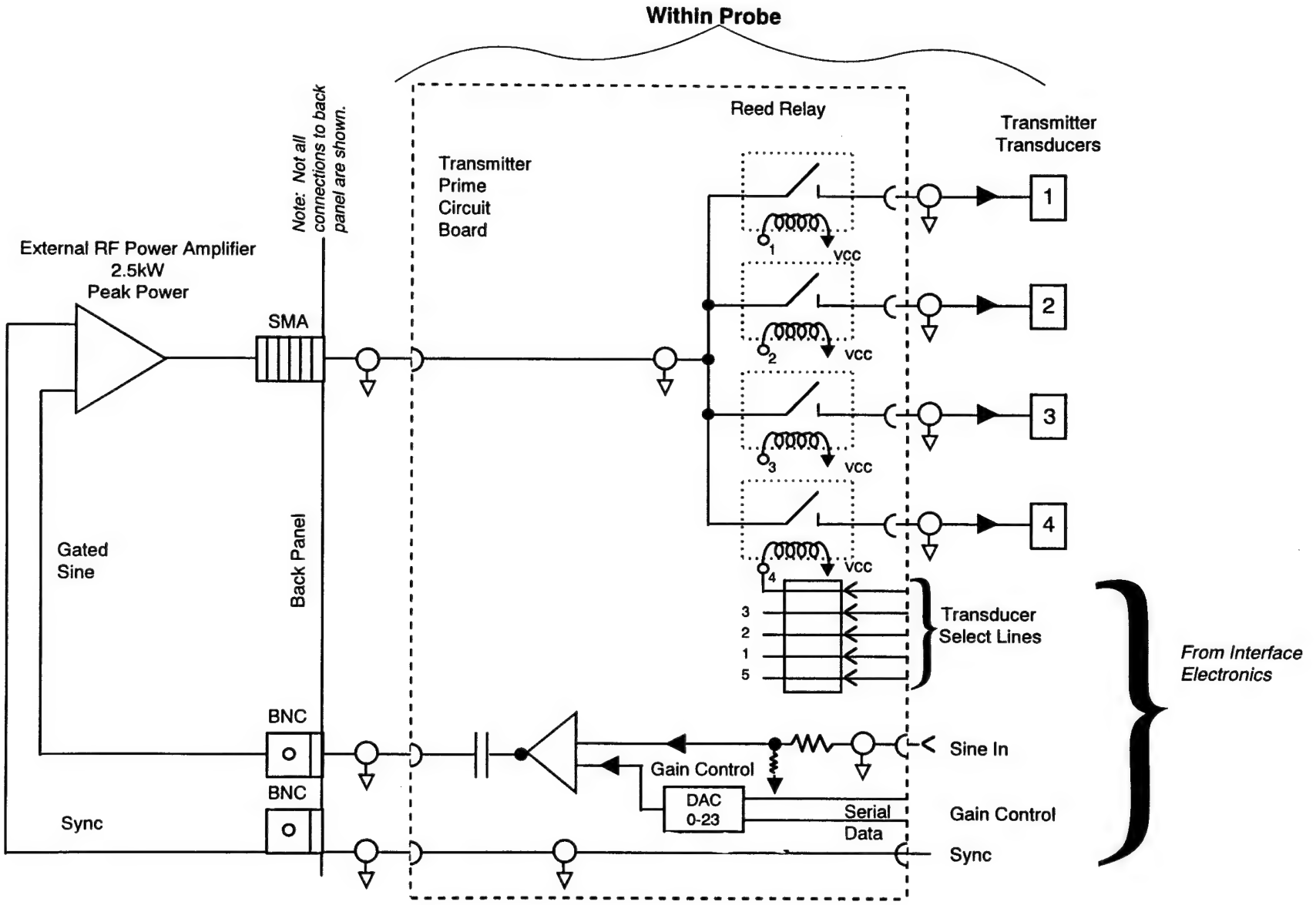

Figure B-1. BUDI Transmitter Subsystem Block Diagram

- Center Frequency: 5.0 ± 0.2 MHz
- Fractional Bandwidth (-6 dB): Greater than 40% (4 to 6 MHz)
- Efficiency: > 10%
- Peak Electrical Power Capability: 2.5 kW peak @ 1.0% Duty Cycle
- Beam Profile (-6 dB re Acoustic Axis): Diverging

Figure B-2. Key Requirements

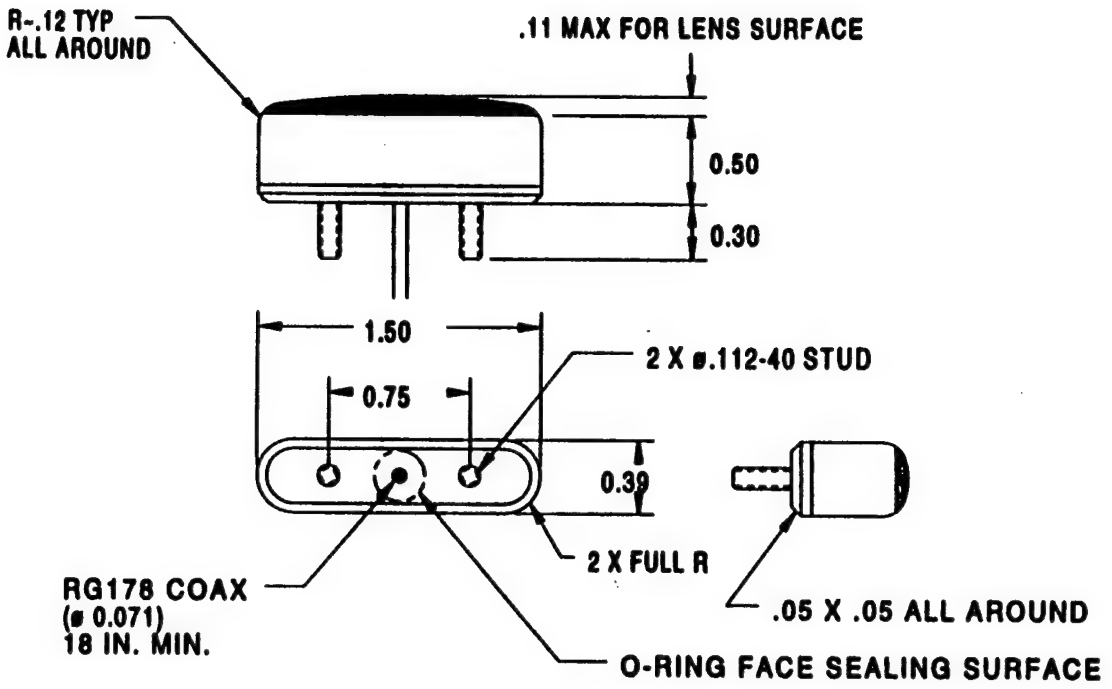

Figure B-3. Transmit Transducer

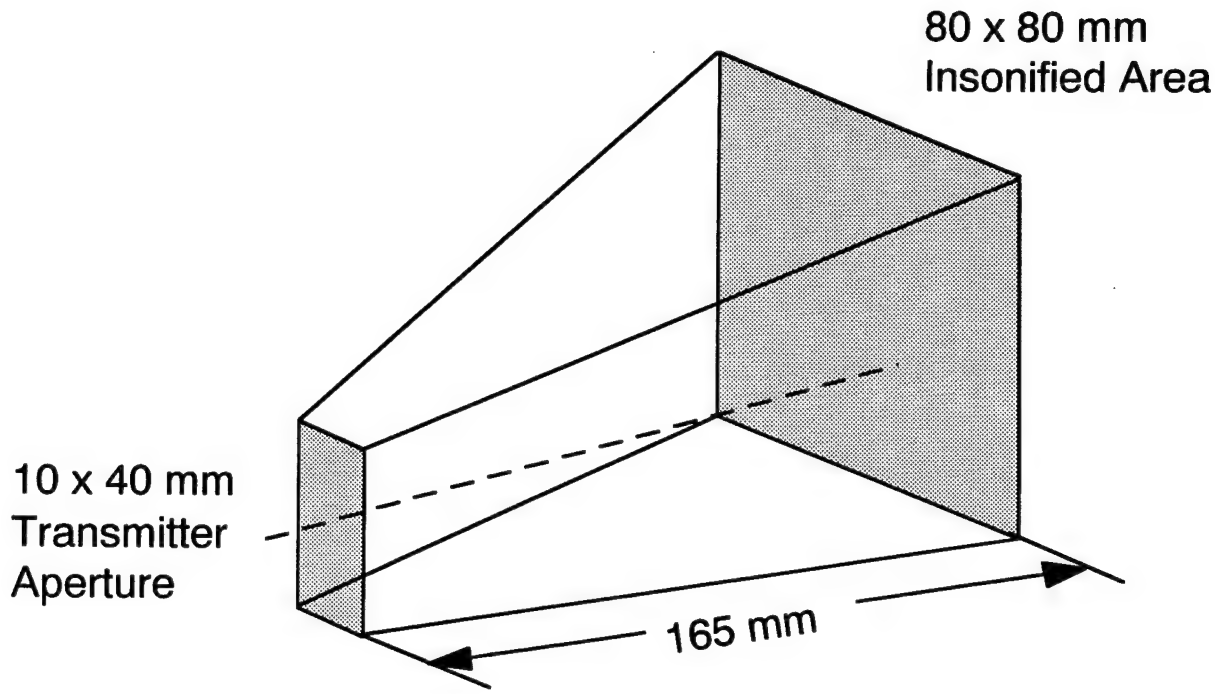

Figure B-4. Narrow Rectangular Transmitter Mnimizes Probe Assembly Diameter

APPENDIX C
ACOUSTIC LENS

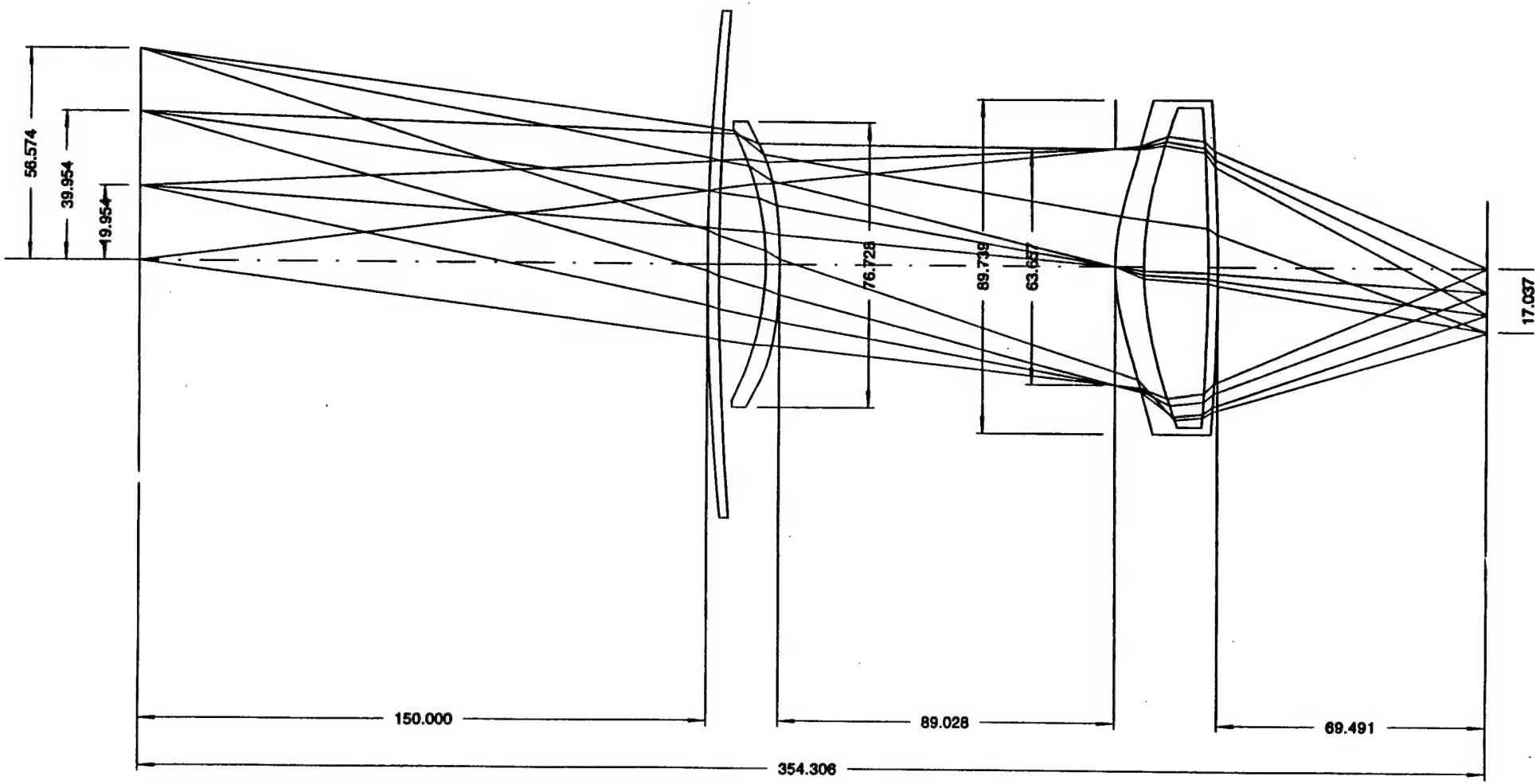

Figure C-1. BUDI Acoustic Lens

		Requirements	Predicted Performance
Nominal Operating Wavelength		300 μm	√
Wavelength Range		250 μm - 375 μm	√
Object Range		0 - 15 cm	√
Object Size		100 mm @ 10 cm Range	80 mm x 80 mm Square 113 mm Diagonal
Element 1 Clear Aperture		-	67 mm x 67 mm Square
Footprint on Body		Minimize	√
Focal Plane Size		25.6 mm x 25.6 mm	√
Length		Minimize	204 mm - 354 mm
Blur size: (85% Encircled Energy)	On-Axis Edge of FOV Corner of FOV	0.90 mm 1.25 mm -	1.08 mm 1.10 mm 1.24 mm
F-Number		1.0	1.23
Magnification		-	0.32

Figure C-2. Acoustic Lens Requirements

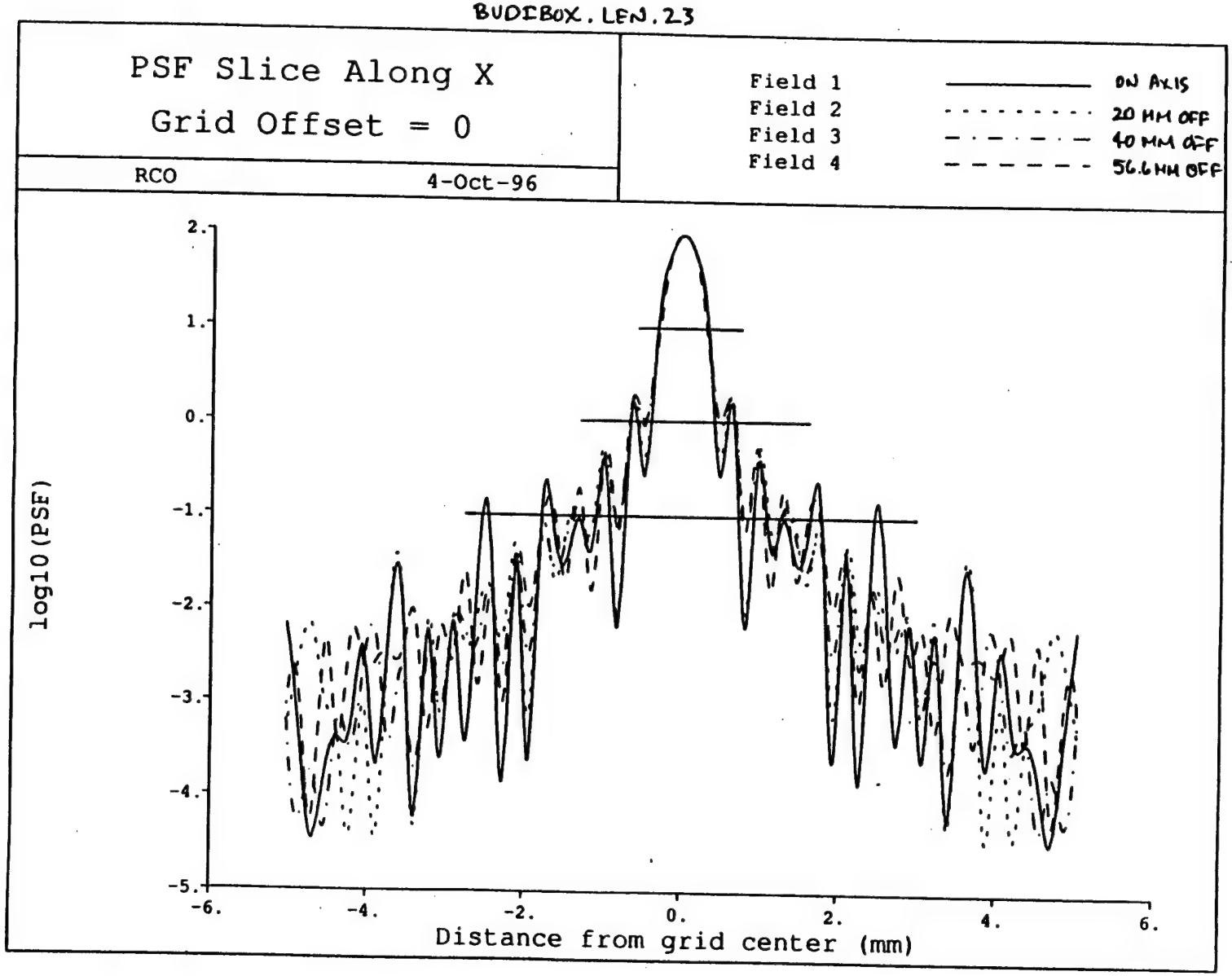

Figure C-3. Acoustic Lens Point Spread Function (Beam Pattern)

Field Position	Magnitude Relative to Central Maximum		
	10%	1%	0.1%
On-Axis	0.64 mm	1.28 mm	5.04 mm
Edge of Field (40 mm off-axis)	0.64 mm	1.28 mm	3.63 mm
Corner of Field (56.6 mm off-axis)	0.64 mm	1.28 mm	3.63 mm

Figure C-4. Extent of Point Spread Function

- **Number of Elements vs. Field-of-View**
  - **2 Elements Provide Diffraction Limited Performance Across 113 mm FOV**
- **Lens Diameter vs. PSF, f/# and Collecting Aperture**
  - **Reduced Lens Diameter from 83.4 mm to 67 mm Square**
    - **PSF Performance Uncompromised: On and Off Axis**
    - **f/# Increased from 1.0 to 1.23**

Figure C-5. Acoustic Lens Key Trades

APPENDIX D
TRANSDUCER HYBRID ASSEMBLY (THA)

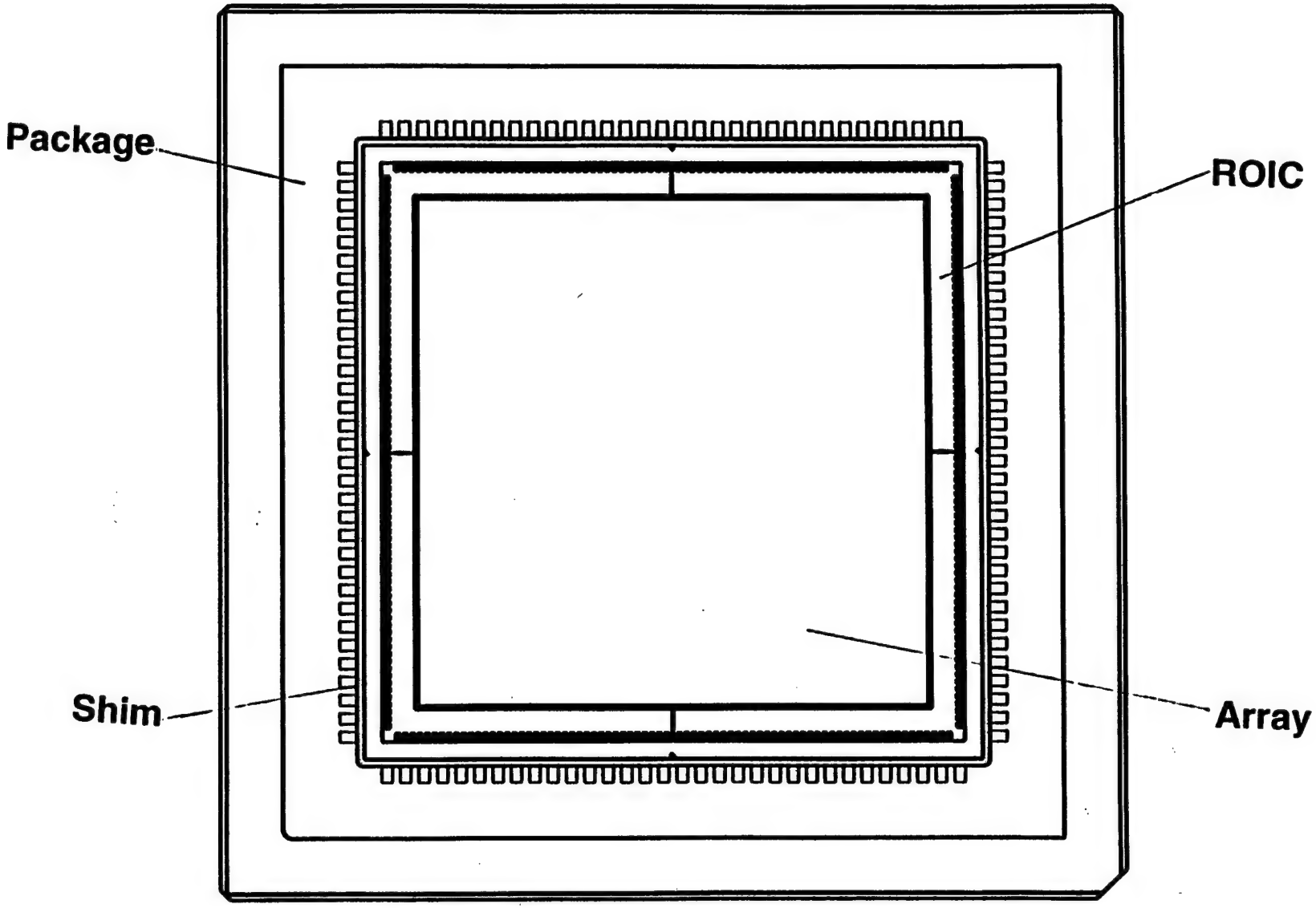

Figure D-1. Transducer Hybrid Assembly: Plan View

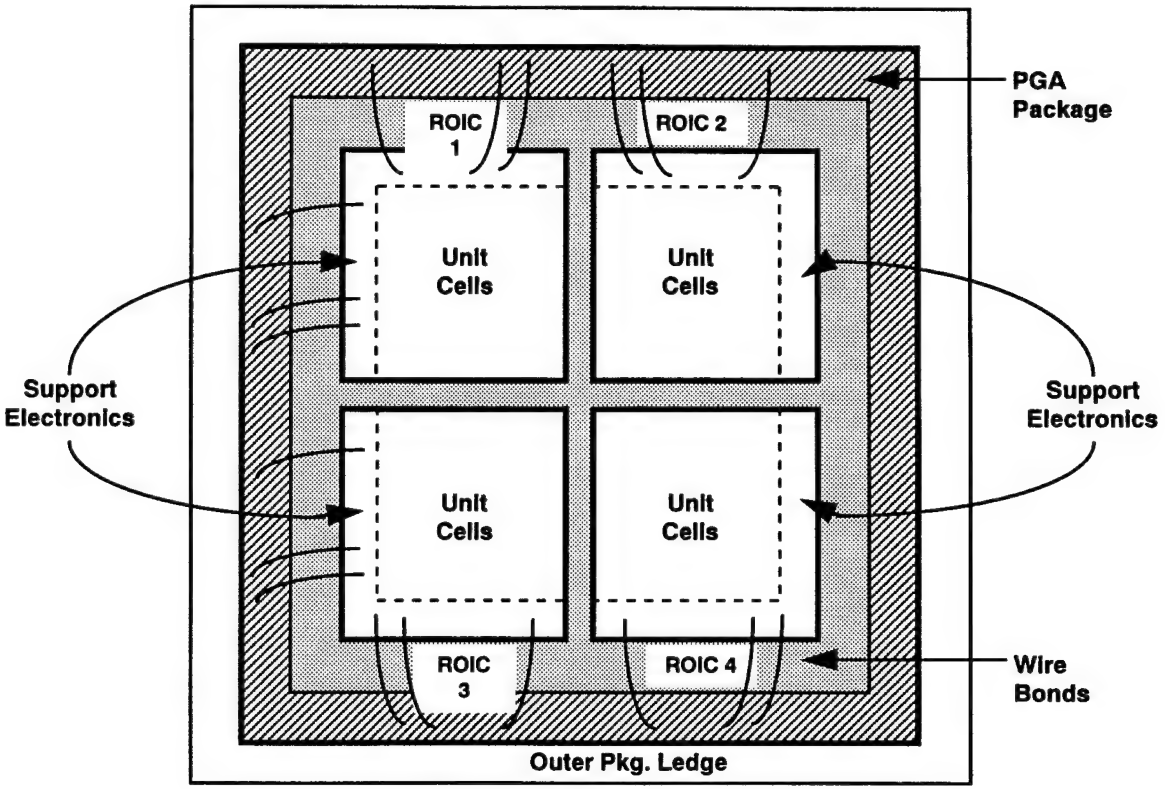

ROICs - 4 per Package
Two-Side Buttable
64 x 64 Unit Cells

Figure D-2. Packaged ROICs: Top View

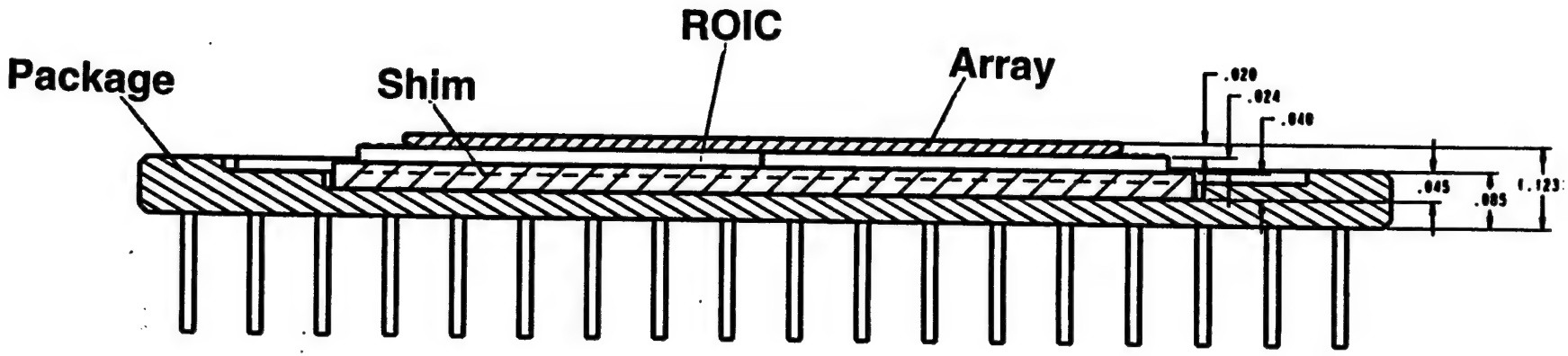

Figure D-3. Transducer Hybrid Assembly: Cross Section

APPENDIX E
ARRAY

	Requirements	Prediction
Physical		
Array Size	128x128 Elements (16,384 total)	OK
Element Size	0.18 mm x 0.18 mm	OK
Center to Center Spacing	0.2 mm	OK
Acoustical		
Center Frequency	5.0 $\pm$ 0.25 MHz	OK
-6 dB Bandwidth	2MHz (4.0 to 6.0)	OK
Pressure Sensitivity	> -220 dB re 1V/mPa	OK
Crosstalk	< -30 dB re Nearest Neighbor	OK

Figure E-1. TransducerArray Specifications

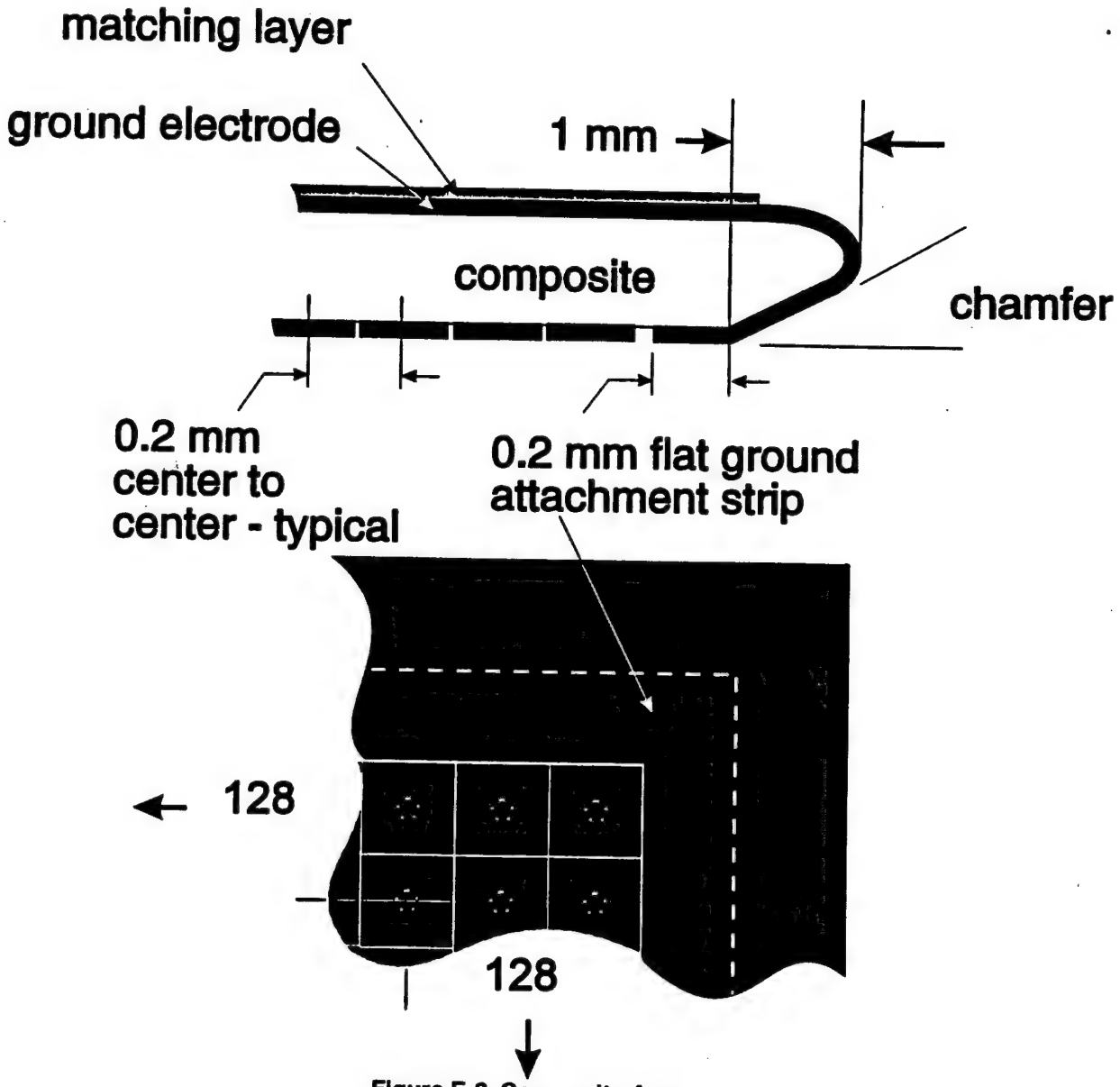

Figure E-2. Composite Array

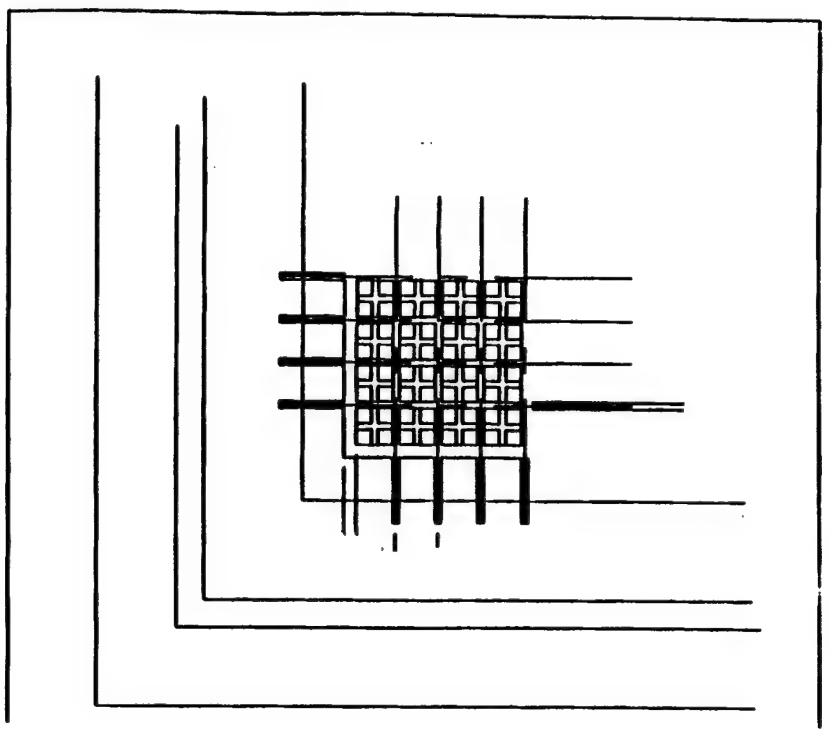

Figure E-3. Detail of Composite Array Elements

APPENDIX F
ROIC

- **64 x 64 Array of Input Cells on 200 μm Pitch**
- **ROIC will be 2-Side Buttable to Allow Construction of a 128 x 128 FPA**
- **Each Input Cell Contains:**
  - *Input Amplifier*
  - *5 Banks of 4 Storage Cells*
  - *Column Driver*
- **4 On-Chip, 10 MHz Output Buffers Drive Data Off Chip**
- **Clock Generator Generates Input Sample Clocks and Output Readout Clocks from Single External Clock**
- **Bias Generator Generates Biases for Amplifiers and Biases Necessary for the Analog Signal Chain**
- **External RF Test Signal may be Applied to any Cell**

Figure F-1. BUDI ROIC Description

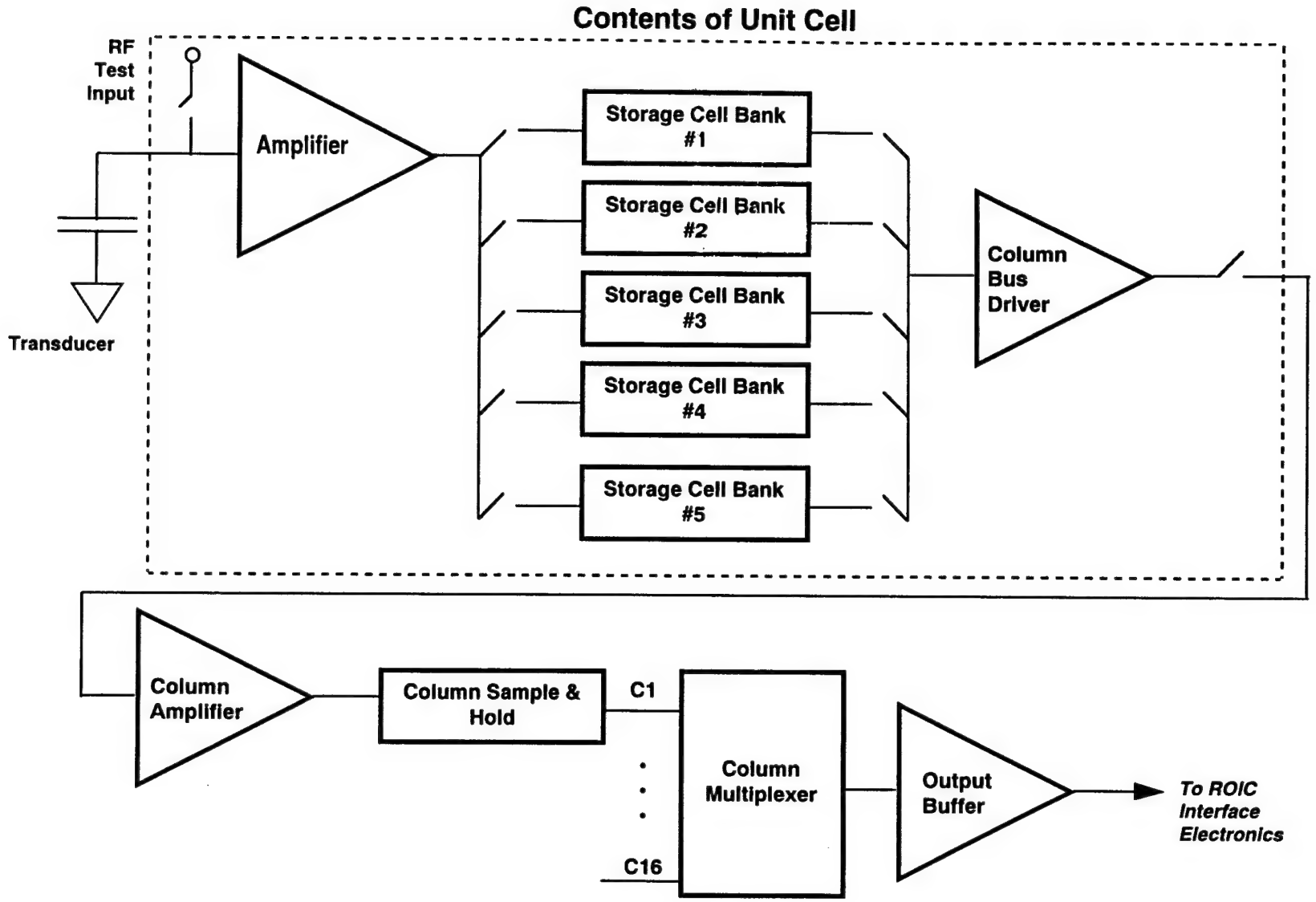

Figure F-2. BUDI ROIC Signal Chain Block Diagram

	Requirements	*Prediction*
Array Size:	64 x 64	√
Pixel Pitch:	200 μm	√
Instantaneous Dynamic Range:	> 60 dB	√
Max Power:	2 W	0.2
Operating Temperature Range:	15°C - 50°C	√
Bandpass Cutoff Frequency:	> 10 KHz	√
Bandpass Cutoff Frequency:	> 8 MHz	√
Gain States:	10, 100	2, 20, 200
Gain Accuracy:	± 30%	± 10%
Gain Variation: (Pixel to Pixel Standard Deviation)	5%	√
Distortion:	- 60 dB THD w/2V Swing	√
Input Referred Noise at Max Gain:	5 nV/rtHz	6.6nV/rtHz
Sample and Hold Number:	16 Minimum	20
Maximum Sample Frequency:	20 MHz	√
Piezoelectric Detector Minimum Series Capacitance:	0.15 pF over Frequency Range	√

Figure F-3. BUDI ROIC Performance Specification

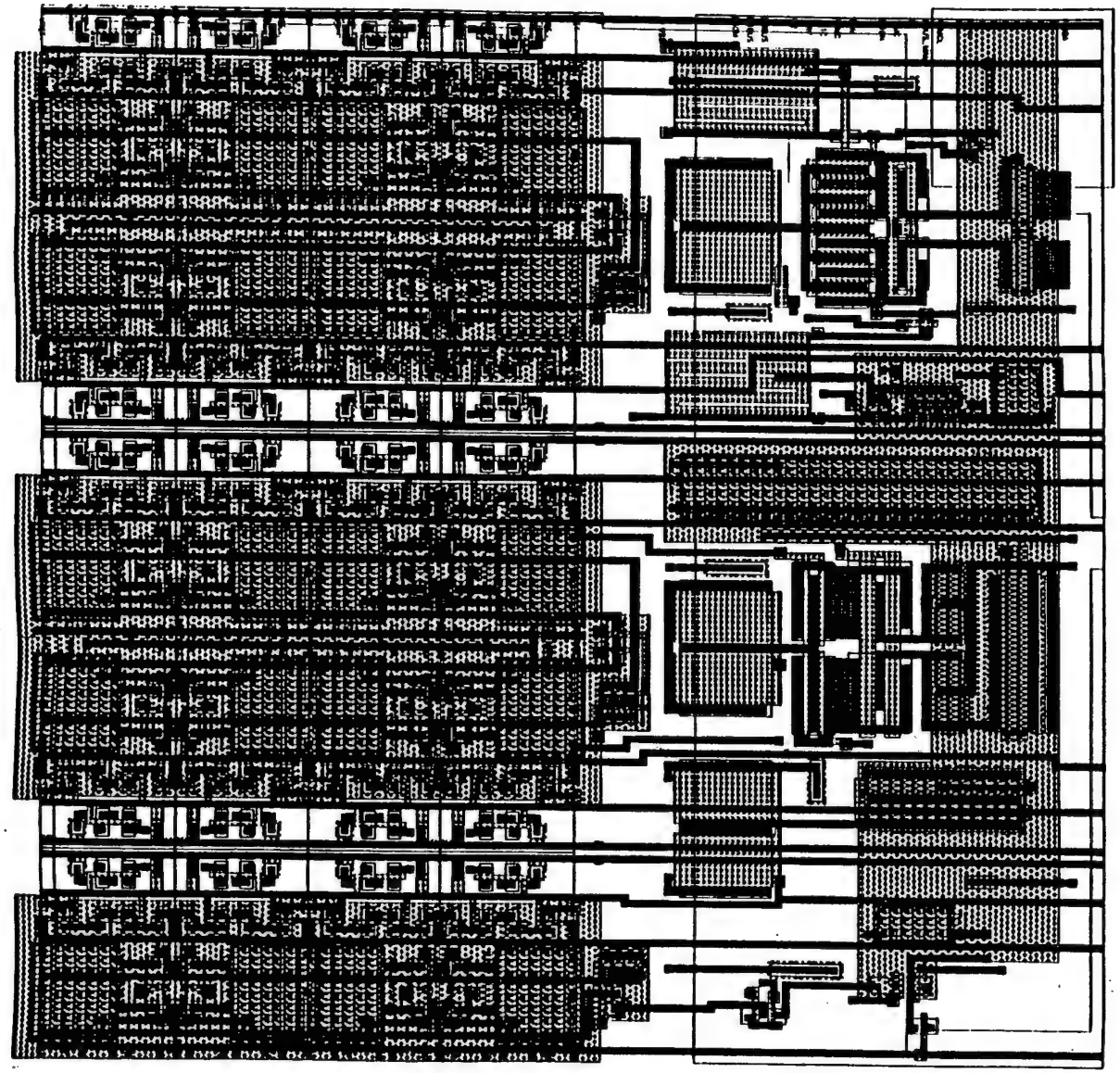

Figure F-4. ROIC Unit Cell Layout

- **Mode 1 - In Phase/Quadrature Detection**
  - *Sample Clocks Obtain I, -I, Q, -Q*
  - *Up to 5 Planes Collected per Readout Frame*
- **Mode 2 - Waveform Sampling**
  - *Employs Sample and Hold Storage*
  - *Up to 20 Samples per Readout Frame*

Figure F-5. ROIC Data Collection Modes

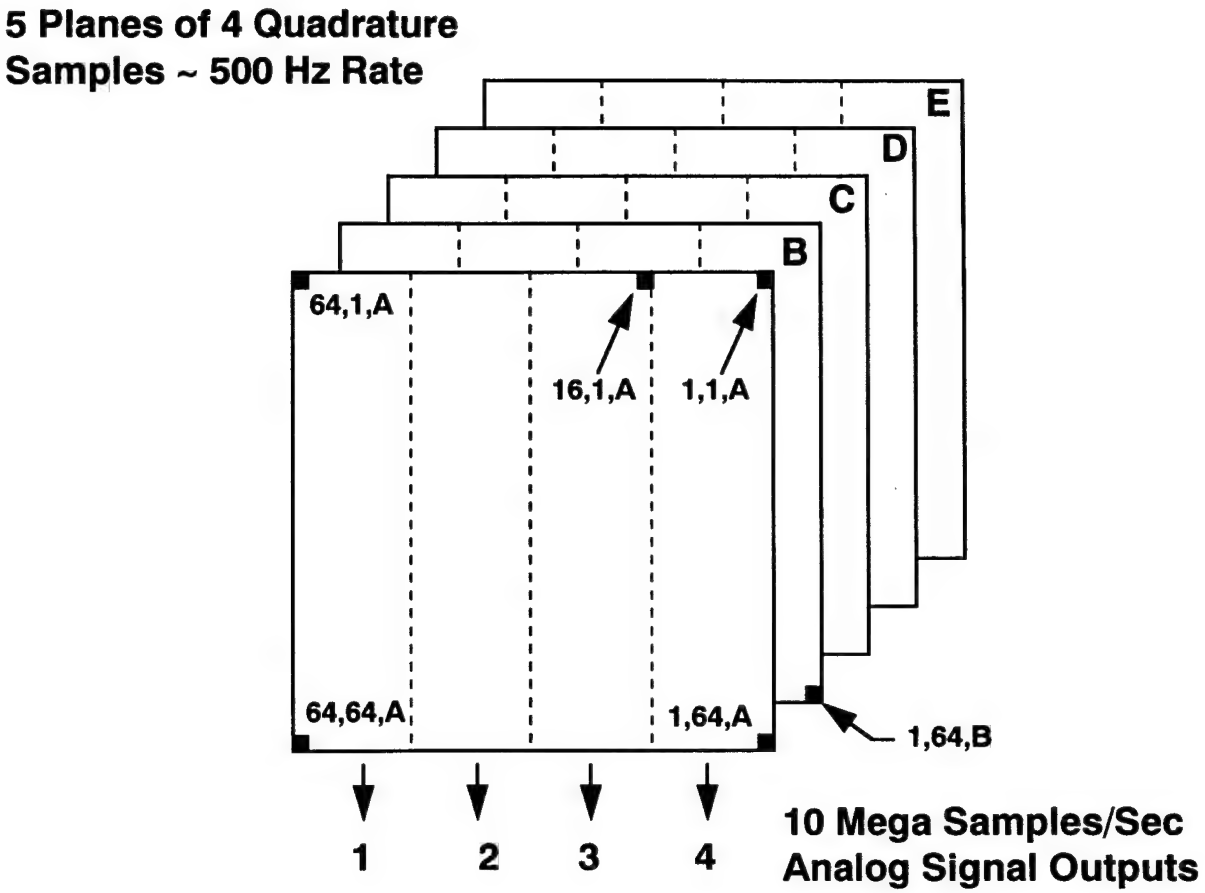

Figure F-6. Pixel Data Format for Each of Four ROICs

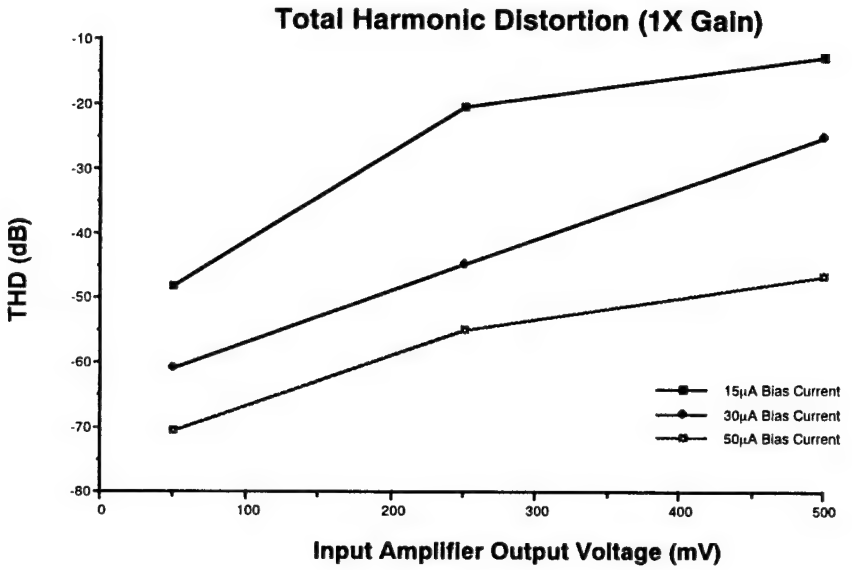

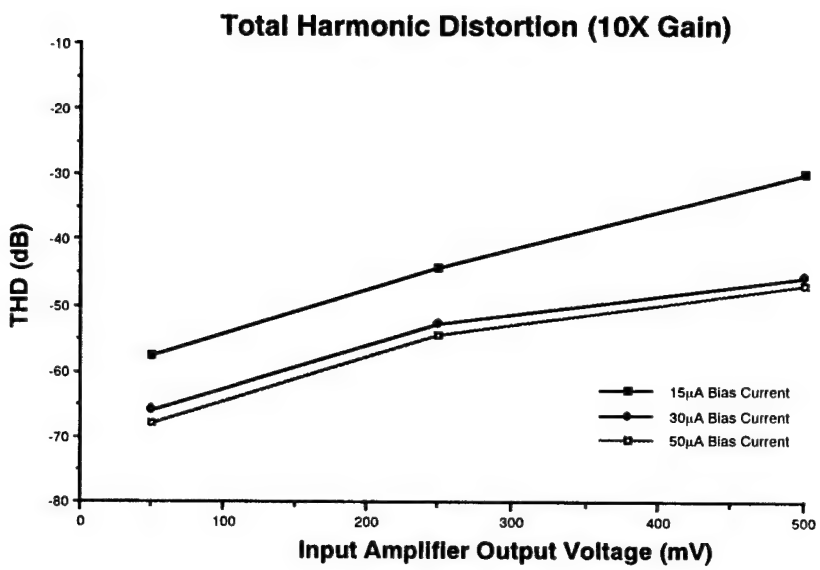

Minimizing Total Harmonic Distortion Dictates Operation @ 50 μA Bias

Figure F-7. Input Amplifier Total Harmonic Distortion

Gain	Bias Current	Bandwidth	Spot Noise	Wideband Noise
10X (Highest Sensitivity Case)	15	12 MHz	8.9 nV/rtHz	31 μV
	30	15 MHz	7.5 nV/rtHz	29 μV
	50	17MHz	6.6 nV/rtHz	27 μV
1X	15	30 MHz	8.9 nV/rtHz	49 μV
	30	45 MHz	7.5 nV/rtHz	50μV
	50	70 MHz	6.6 nV/rtHz	55 μV

Noise and Bandwidth Performance Dictate Amplifier Operation @ 50 μA Bias

Figure F-8. Input Amplifier Wideband Noise

Wideband Noise (Input Referred)	Noise After Signal Av'g	Max SNR	Peak Input Voltage Swing	Input Amp Gain	Column Amp Gain	Output Amp Gain	Peak Output Voltage Swing	THD
27 μV	8.5 μV	832 (58dB)	± 5 mV	10 (± 50 mV)	2 (± 50 mV)	10	± 1 V	- 68dB
55 μV	17.4 μV	4,064 (72dB)	± 50 mV	1 (± 50 mV)	2 (± 50 mV)	10	± 1 V	-70 dB
55 μV	17.4 μV	40,640 (92dB)	± 500 mV	1 (± 500 mV)	2 (± 500 mV)	1	± 1 V	-47 dB

Figure F-9. ROIC Electrical Operating Modes

- **Crosstalk Mechanisms**
  - *–RF Coupling Between Cells*
  - *–Power Supply Coupling*

Cell-to-Cell Crosstalk

Input Amplifier Gain	***Best***	***Typical***	***Worst***
1X	**-110dB**	**-84dB**	**-80dB**
10X	**-86dB**	**-68dB**	**-64dB**

Predicted Crosstalk Levels Support Full Dynamic Range

Figure F-10. ROIC Cell-to-Cell Crosstalk

APPENDIX G
SYSTEM ELECTRONICS

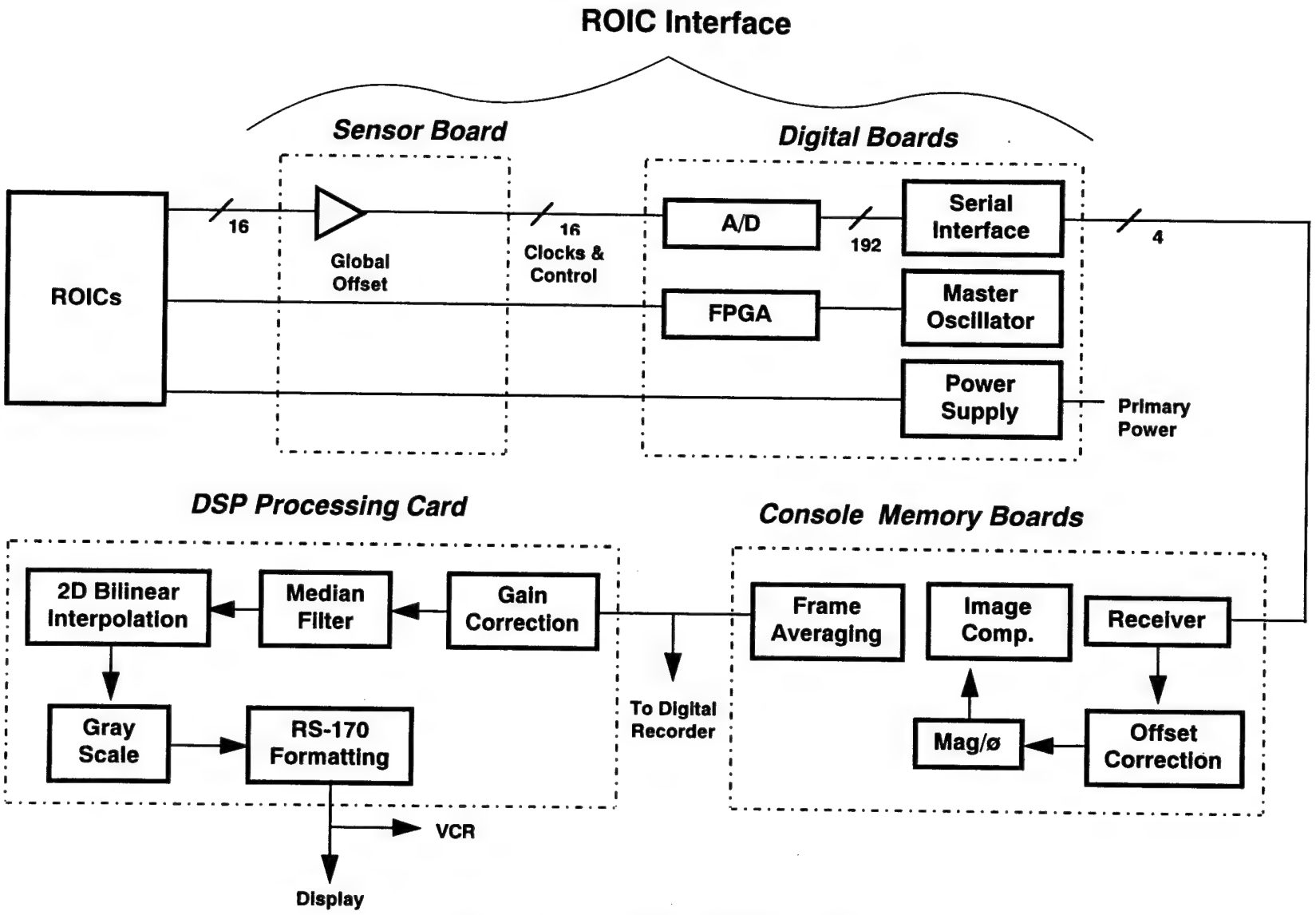

Figure G-1. BUDI Signal Processing Path

- **Interfaces ROICs to Console Board**
- **16 Parallel Channels**
- **12 Bit Digitization**
- **10 M Samples/Sec per ROIC Channel**
- **Controls ROIC Readout Modes**
  - *Clocks*
  - *Biases*
  - *Multiplexing*
- **Transmit High Speed Data (300 M Bytes/Second)**
- **ROIC Control Programming Downloaded from Host Computer**
- **Provide ROIC and THA Test Capability**

Figure G-2. ROIC Interface Requirements

- **Receive High Speed Data (300 M Bytes/Second)**
- **Execute Algorithm Functions**
  - *–Gain Correction*
  - *–Offset Correction*
  - *–Magnitude Calculation*
  - *–Phase Calculation*
- **Compose Image Data**
- **Buffer Image Data for Digital Recording and Cineloop**
- **Transmit Image Data to Processing Card**

Figure G-3. Console Board Requirements

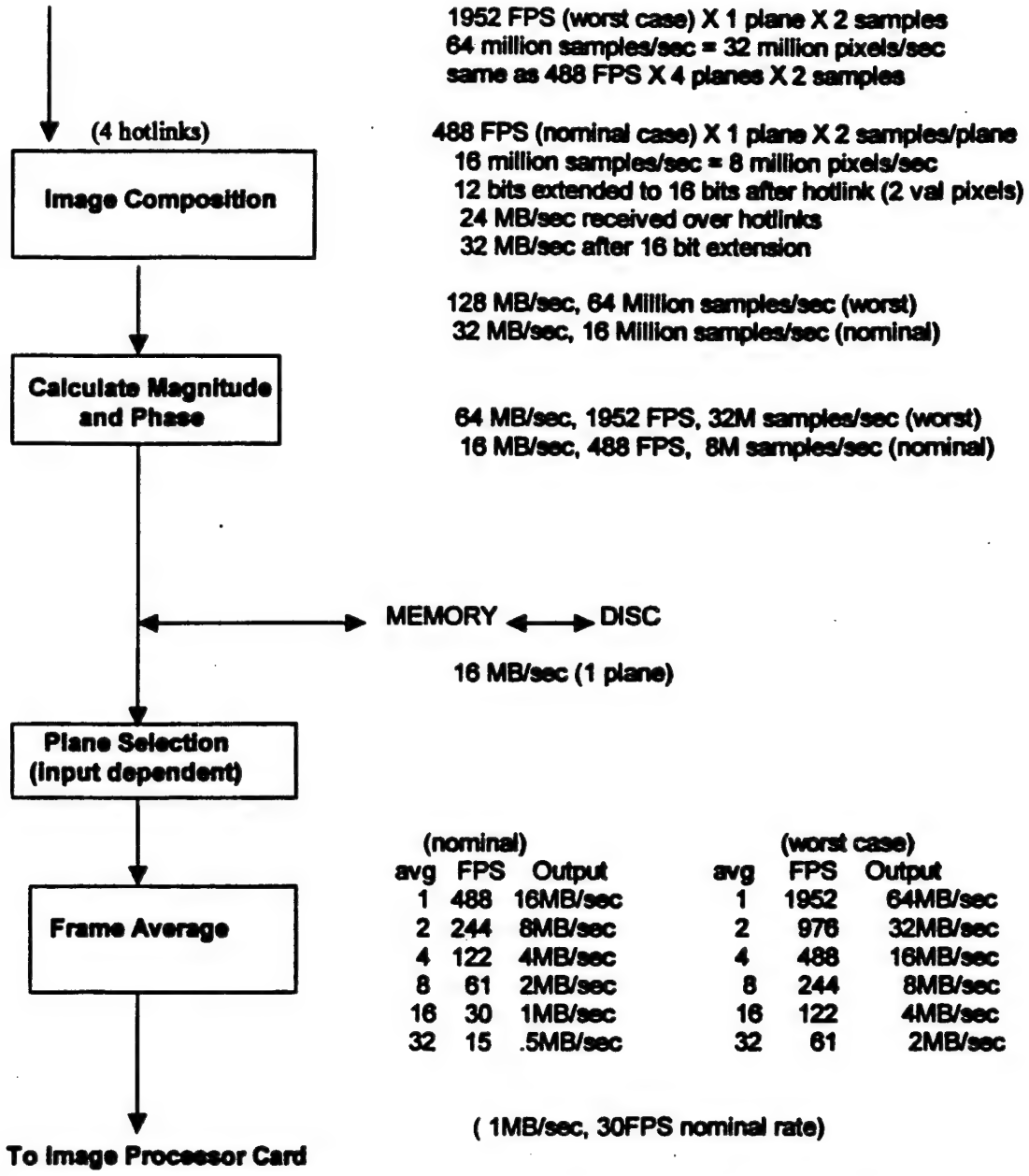

Figure G-4. Console Card Algorithms Quadratuve Sampling Mode

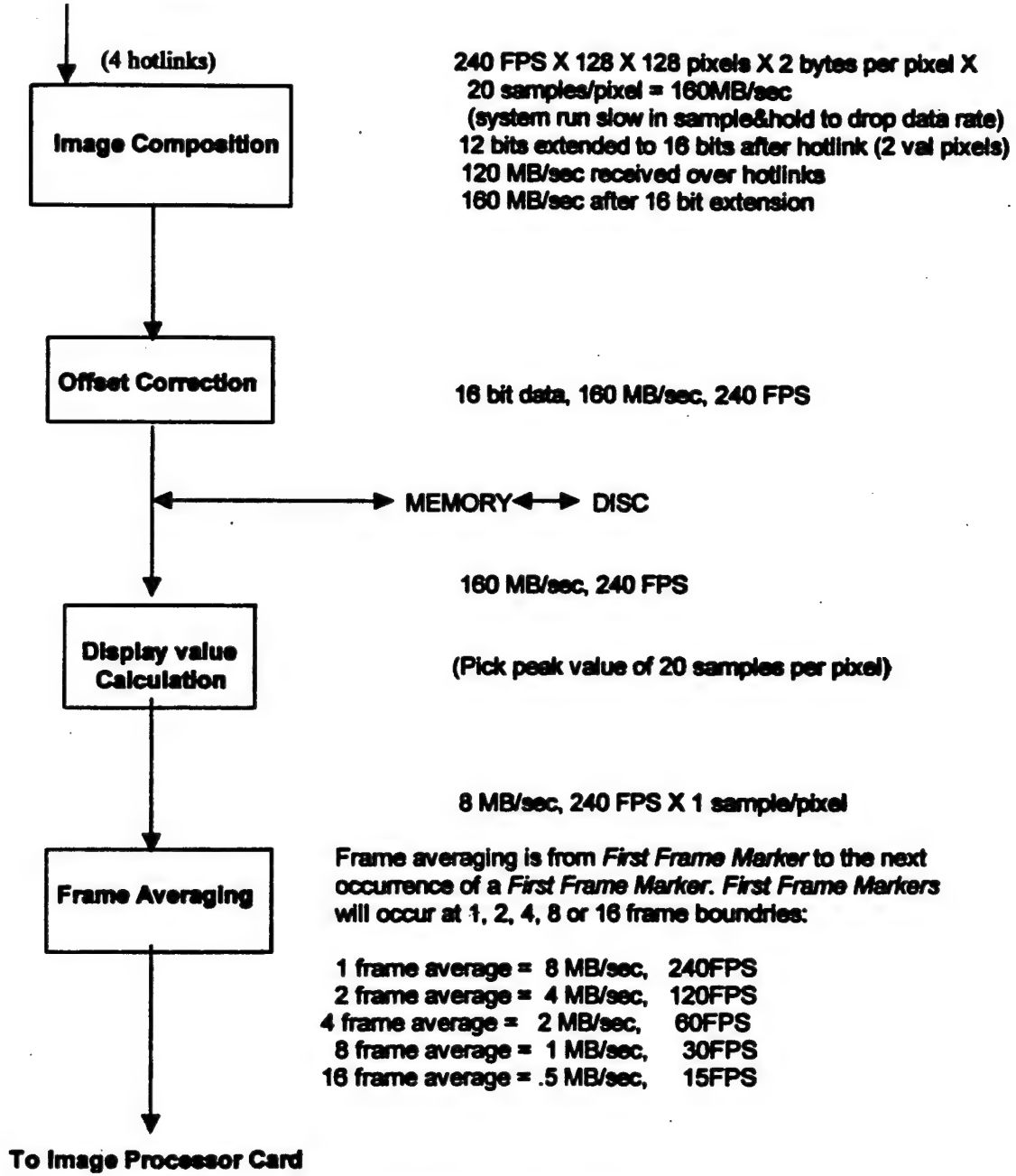

Figure G-5. Console Card Algorithms Digital Sampling Mode

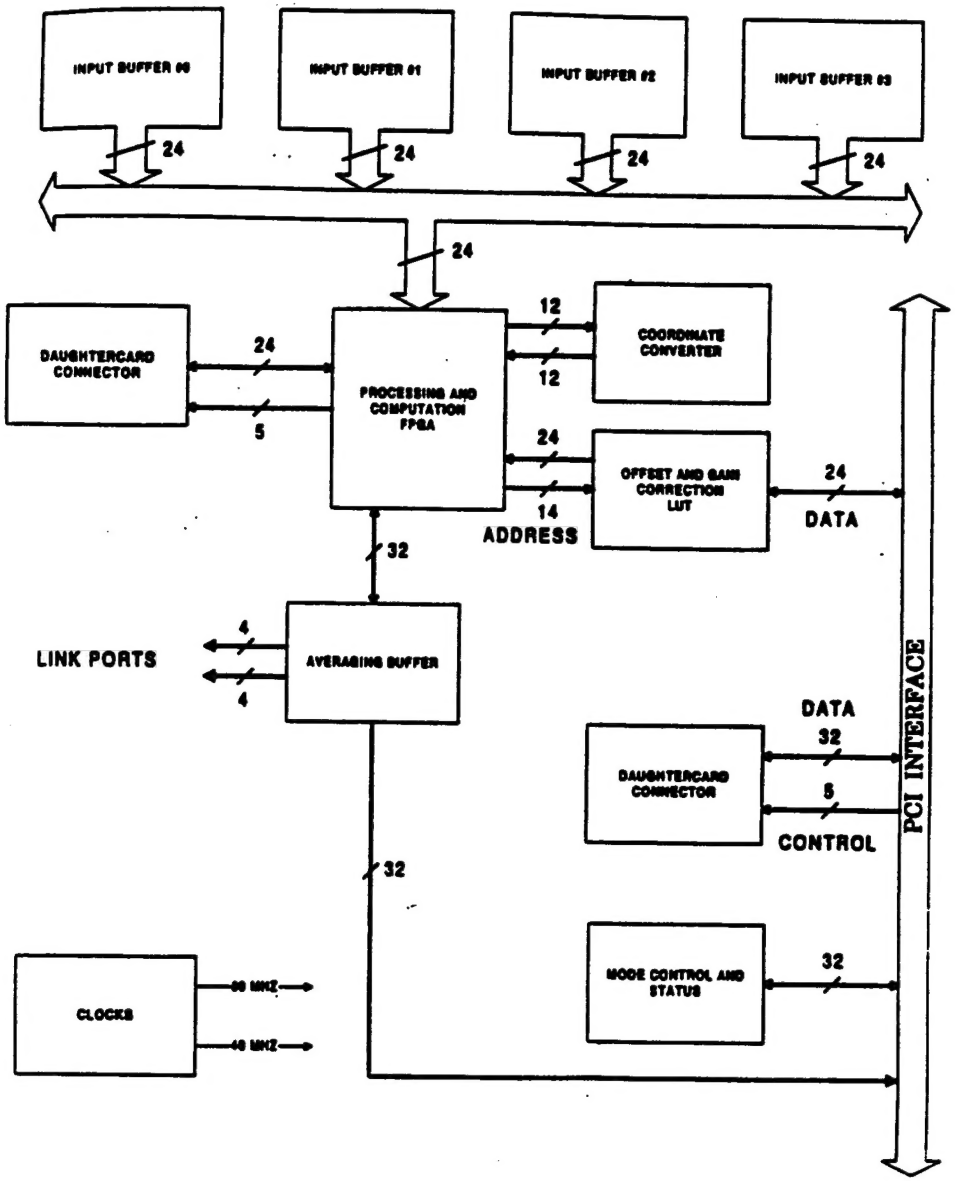

Figure G-6. Console Board Hardware Block Diagram

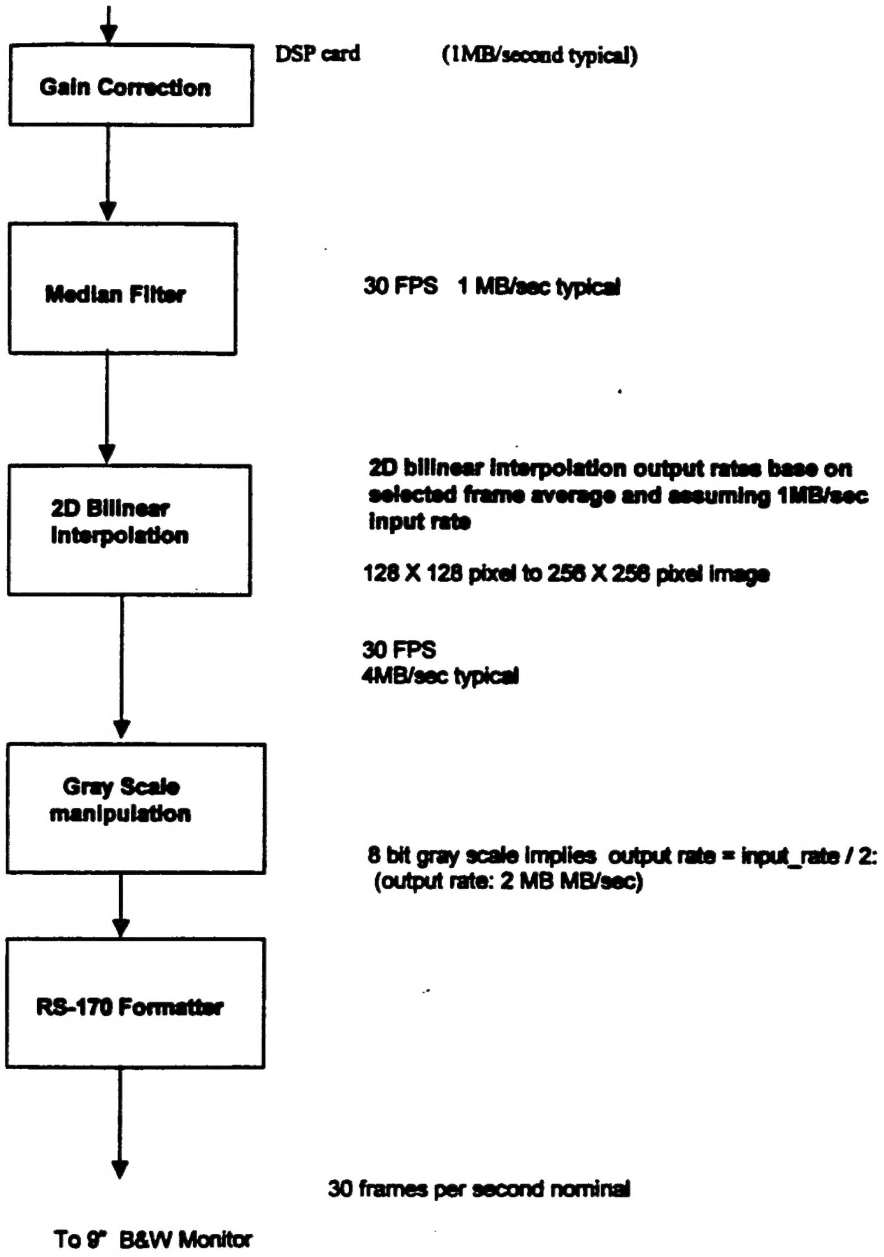

Figure G-7. Image Processor Card Algorithms

APPENDIX H
BUDI LDS SOFTWARE

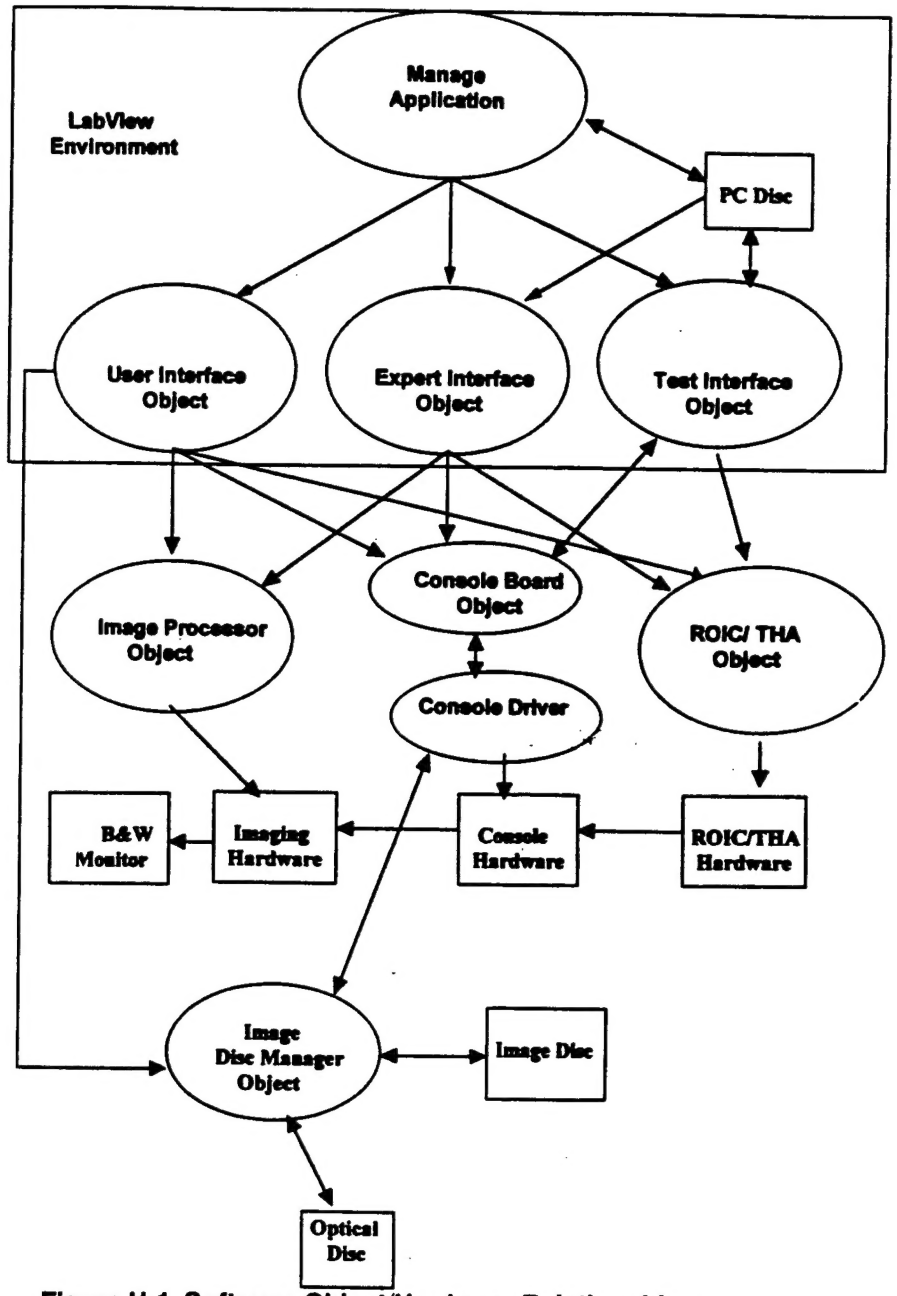

Figure H-1. Software Object/Hardware Relationships